Universidade de Aveiro Departamento de Electrónica, Telecomunicações e Informática,
2016

Inês do Vale Marques Oliveira

Equalização Digital da Dispersão Cromática em Sistemas de Transmissão Óticos Coerentes

Digital Chromatic Dispersion Equalization in Optical Coherent Transmission Systems

Inês do Vale Marques Oliveira

Equalização Digital da Dispersão Cromática em Sistemas de Transmissão Óticos Coerentes

Digital Chromatic Dispersion Equalization in Optical Coherent Transmission Systems

Dissertação apresentada à Universidade de Aveiro para cumprimento dos requisitos necessários à obtenção do grau de Mestre em Engenharia Electrónica e Telecomunicações, realizada sob a orientação científica do Professor Doutor Armando Nolasco Pinto, Professor Associado do Departamento de Electrónica, Telecomunicações e Informática da Universidade de Aveiro, e sob a co-orientação científica do Doutor Fernando Pedro Pereira Guiomar, Investigador do Instituto de Telecomunicações.

Dissertation submitted to *Universidade de Aveiro* to accomplish the requirements for obtaining a Master's degree Electronics and Telecommunications Engineering, performed under the scientific supervision of Professor Doctor Armando Nolasco Pinto, Associate Professor in *Departamento de Electrónica, Telecomunicações e Informática* from *Universidade de Aveiro*, and under the scientific co-supervision of Doctor Fernando Pedro Pereira Guiomar, Researcher from *Instituto de Telecomunicações*.

Work dedicated to my parents and brother.

the jury

president

Professor Doutor José Ferreira da Rocha
Full Professor, *Universidade de Aveiro*

examiners committee

Professor Doutor Paulo Sérgio de Brito André
Associate Professor with Aggregation, *Universidade de Lisboa*

Professor Doutor Armando Humberto Moreira Nolasco Pinto
Associate Professor, *Universidade de Aveiro*

acknowledgements

Firstly, I want to thank my parents for giving me the opportunity of taking this master degree, and for supporting me the whole time. My mother for her wonderful advices, and my father for believing in me always.
Secondly, I want to thank my friends, also colleagues, for their fellowship and for their help during the last six years. With them on my side, this stage of my life became much easier. Special thanks to David.
Finally, I want to thank my supervisor for his availability and patience, and the people from *Instituto de Telecomunicações* who helped me and advised me during the realization of this dissertation.

palavras-chave

deteção coerente, dispersão cromática, fibra ótica, modulação por deslocamento de fase e quadratura, processamento digital de sinal, sistema de comunicação ótico

resumo

A crescente procura de largura de banda tem obrigado a área de comunicações óticas a explorar diferentes soluções, de forma a evitar a "crise de capacidade" [1]. O investigadores têm trabalhado no sentido de atingir o equilíbrio entre os vários compromissos, repensando a forma como o sinal ótico é enviado e recebido, para que a perda de informação seja mínima ao longo do canal de propagação. No início desta década, começaram a ser adotados formatos de modulação avançada, os quais apresentam elevada eficiência espetral, bem como deteção coerente, que permite extrair a informação da amplitude e da fase do campo ótico. Estas técnicas são complementadas pelo pós-processamento digital de sinal, que é atualmente muito importante na mitigação das distorções do sinal e imperfeições do recetor. As distorções do sinal podem ser causadas, por exemplo, pela dispersão cromática na fibra.

Esta dissertação engloba o estudo e simulação de um sistema de transmissão coerente PM-QPSK, bloco-a-bloco, fazendo uma abordagem detalhada dos conceitos supramencionados. O sistema foi então simulado na presença de dispersão cromática e de ruído, alternada e simulataneamente. Os resultados mostram que o sinal recebido apresenta uma distribuição quase Gaussiana em todos os casos. Com vista a recuperar o sinal transmitido, e no caso em que só se considerou o efeito da dispersão cromática, aplicou-se um filtro linear de resposta impulsional inversa à da fibra, conseguindo assim uma equalização digital perfeita do sinal recebido. Também foi implementado um filtro adaptado no receptor para minimizar o efeito do ruído, obtendo não uma equalização perfeita, mas ótima.

keywords chromatic dispersion, coherent detection, digital signal processing, optical communication system, optical fibre, quadrature phase-shift keying

abstract The crescent demand on high bandwidth has been compelling the optical communications area to explore different solutions, in order to avoid the "capacity crunch" of the optical fibres [1]. Researchers have been working towards reaching the best tradeoffs balance, rethinking the way as the optical signal is sent and received, so the loss of information is minimum throughout the propagation channel. Advanced modulation formats became adopted in the beginning of this decade, presenting high spectral efficiency, as well as coherent detection, which allows extracting information from the amplitude and phase of the optical field. These techniques are complemented by post-digital signal processing, which is nowadays very important at mitigating signal distortions and receiver imperfections. Those impairments result, for instance, of the chromatic dispersion at the fibre.

This dissertation covers the study and simulation of a PM-QPSK transmission system, block-by-block, approaching in detail the concepts mentioned above. The system was then simulated with chromatic dispersion and with noise, alternately and simultaneously. The results show that the received signal presents an almost Gaussian distribution in every case. In order to retrieve the transmitted signal, and in the case that only chromatic dispersion's effect was considered, a linear filter was applied with an inverse impulse response of the fibre, achieving such a perfect digital equalization of the received signal. A matched filter was also implemented in the receptor to minimize the noise effect, obtaining not a perfect equalization, but an optimal one.

Contents

List of Acronyms

ADC	analog-to-digital converter
AM	amplitude modulation
ASE	amplified spontaneous emission
ASK	amplitude-shift keying
AWG	arbitrary waveform generator
AWGN	additive white Gaussian noise
BER	bit error rate
CD	chromatic dispersion
CMA	constant-modulus algorithm
DAC	digital-to-analog converter
DCF	dispersion-compensating fibre
DSF	dispersion-shifted fibre
DSP	digital signal processing
DWDM	dense wavelength-division multiplexing
EBW	excess bandwidth
EDFA	Erbium doped fibre amplifier
FDE	frequency-domain equalizer
FEC	forward error correction
FFT	fast Fourier transform

FIR	finite impulse response
FPGA	field-programmable gate array
FSK	frequency-shift keying
GVD	group velocity dispersion
IIR	infinite impulse response
IM/DD	intensity modulation & direct detection
IQ	in-phase & quadrature
ISI	inter-symbol interference
LEAF	large effective area fibre
LFSR	linear feedback shift register
LMS	least mean square
LO	local oscillator
LPF	low-pass filter
MMF	multi-mode fibre
MZ	Mach-Zehnder
NCO	numerically controlled oscilator
NRZ	nonreturn-to-zero
OH	optical hybrid
OOK	on-off keying
OPLL	optical phase-locked loop
OSNR	optical signal-to-noise ratio
PAPR	peak-to-average power ratio
PBC	polarization beam combiner
PD	photodetector

PDF	probability density function
PIN	positive-intrinsic-negative
PM	phase modulation
PMD	polarization mode dispersion
PM-QPSK	polarization-multiplexed quadrature phase-shift keying
PolSK	polarization-shift keying
PRBS	pseudo-random binary sequence
PSD	power spectral density
PSK	phase-shift keying
QAM	quadrature amplitude modulation
QPSK	quadrature phase-shift keying
RF	radio-frequency
RMS	root-mean square
RRC	root raised cosine
RX	receiver
RZ	return-to-zero
SMF	single-mode fibre
SNR	signal-to-noise ratio
SONET	synchronous optical network
SOP	state of polarization
TED	temporal error detector
TX	transmitter
WDM	wavelength-division multiplexing

List of Figures

List of Tables

Chapter 1

Introduction

In a first stage, the first Chapter approaches the motivation followed by the objectives of the current dissertation, in Sections 1.1 and 1.2, respectively. Right after, Section 1.3 has a description of the dissertation structure as well as Section 1.4 has a listing of the major achievements. At last, Section 1.5 presents the state-of-the-art that explores the historical perspective of coherent transmission systems and also explains all the preliminary concepts necessary to understand the PM-QPSK optical transmission systems. Those concepts include modulations formats, coherent detection, and an overview on DSP, highlighting the dispersion equalization.

1.1 Motivation

Optical communications are based on the transmission of information carried by optical signals, which are high-frequency electromagnetic waves. Optical fibre is the more usual medium chosen for the propagation of these waves. Due to its huge bandwidth potential, this type of waveguides quickly became favourite regarding the transmission in telecommunication networks. Thanks to the usage of optical fibres, telecommunication networks have increased their capacity and distance, year after year. This increase aims to respond to the high traffic demand imposed by the society.

Over the last years, optical communications have suffered a fast evolution in terms of transmission technologies and signal detection. Services like cloud computing, file-sharing or high-definition television distribution were prompters of such an evolution because they have demanded a greater amount of data traffic. This data traffic increase meant a bandwidth overloading on the optical links implemented so far. There was the need of restructuring the optical networks as well as the transmitter and receiver.

Previously, the transmission systems were using intensity modulation which were replaced

by quadrature amplitude modulation. The later systems started to implement coherent detection rather than direct detection. Therefore, digital processing of the detected signal became achievable. The post-DSP (*digital signal processing*) allows to equalize the distorted signal often caused by signal propagation [3]. This process increases the score and range of optical links and, consequently, reduces the complexity of optical networks. These reasons together led to consider DSP as a key technology of the present generation optical transmission systems. All those changes allowed the increase of optical channel bit-rates from 10 Gb/s to 40/100 Gb/s [4]. According to the actual researching, it is expected that the next generation systems may support bit-rates of 400 Gb/s and 1 Tb/s per channel.

1.2 Objectives

The main purpose of this dissertation is based on the post-compensation of the received signal in a PM-QPSK transmission system, particularly at CD (*chromatic dispersion*) level. This fact leads to make the proper study of that system, so the objectives also pass through the full understanding of the optical coherent transmission parts: transmitter and receptor as well as the propagation medium, i.e. the optical fibre where CD occurs.

The subject demands then several computer-aided simulations around the propagation of an optical signal IQ-modulated, associated to a numerical model of CD. Those simulations may demonstrate the deterministic behaviour of such phenomenon for any scenario of optical channel: any fibre length, with or without noise. Similarly, the simulations may demonstrate the capability of equalizing the CD by inverting its numerical model, once it is linear. This allows yielding a perfect retrieval of the transmitted signal, in an ideal system.

1.3 Dissertation Structure

The dissertation is divided into five Chapters, plus Appendices. It begins with the current Chapter 1 which introduces the optical coherent transmission systems by doing an historical contextualization and discussing the main concepts associated to the dissertation subject such as modulation formats, coherent detection and digital post-processing. Chapter 2 describes in detail a PM-QPSK optical transmission system. The Chapter 3 contains simulation results, obtained in MATLAB®, from different scenarios of propagation. Those results show the chromatic dispersion and noise effects. Posteriorly, the Chapter 4 focus on solving both undesired effects. It covers the digital equalization and matched filtering applied to the simulations of Chapter 3 and contains the respective results, also using MATLAB®. Finally, Chapter 5 presents the main conclusions about the dissertation and proposals of future work.

1.4 Major Achievements

It is reasonable to enumerate some points as the major achievements of this dissertation:

- Study in detail of PM-QPSK optical transmission systems;
- Proof of the signal Gaussianization in the presence of chromatic dispersion and in the presence of white noise;
- Implementation of a digital filter for chromatic dispersion equalization and noise filtering.

1.5 State-of-the-art

Research and development of optical fibre communication systems started in the second half of the 60s. Those systems were characterized by using intensity modulation of semiconductor lasers as well as photodiodes of square-law detection of the optical signal transmitted through the fibre. This combination, designated by IM/DD (*intensity modulation & direct detection*) scheme, became the receiver sensitivity independent of carrier phase and SOP (*state of polarization*) of the incoming signal [5].

In 1970, DeLange [6] proposed, for the first time, a coherent optical communication system using heterodyne detection, but it was not successful against the IM/DD scheme. Later, in 1980, two scientific teams, Okoshi and Kikuchi [7], and Fabre and LeGuen [8], found an advantage on optical heterodyne detection over direct detection. Both independently demonstrated precise frequency stabilization of semiconductor lasers. There was the need of narrowing their spectral linewidths since they caused a random carrier phase fluctuation due to their large phase noise [5]. That contributed a lot for spreading the coherent systems over the optical communications field. While in IM/DD scheme was no need of adaptive control, in the coherent scheme it was necessary feedback the system with carrier phase and SOP. That meant the configuration of coherent systems was more complicated than IM/DD systems. The most complex aspect in a coherent receiver was the fact of synchronizing the phases of the incoming and the LO (*local oscillator*) signals. This required very complex and expensive hardware such as OPLL (*optical phase-locked loop*) in addition to lasers with high spectral purity [9]. Even so, there was more advantages related to the coherent scheme, e.g. the use of the carrier phase to modulate the incoming signal. During 80's decade, coherent detection was seen as a potential implementation. It increased the propagation range due to the better sensibility of the receptor [10]. With the rising of optical amplifiers, at the beginning of the 90s, the coherent detection has lost its potential and became second plan.

During the first 00's decade, the main concern at optical communications field was about optimization of the spectral efficiency. The chosen format to modulate the optical signal started to be relevant for the transmission optimization. The motivation led to find a meeting point between the ever-increasing bandwidth demand and multi-level modulation formats [11]. Coherent technologies emerged again later in the history, with the transmission capacity increase [5]. The demonstration of digital carrier-phase estimation in coherent receivers in 2005 stimulated a widespread interest in that subject [12]. Such a receiver added the fact of enabling the employment of various modulation formats such as M-ary phase-shift keying (PSK) and quadrature amplitude modulation (QAM) similar to radio communications [5].

Below, it is presented the table 1.1 describing the evolution of the optical systems, sectioning it according to the technologies used [2]. By observing the table, it is possible to conclude the evolution followed the best relation between the several factors, such as low attenuation, low cost, high range and high bit-rate.

Generation	**First**	**Second**	**Third**	**Fourth**	**Fifth**
Fibre Innovation	MMF	SMF	DSF	SMF+DCF	SMF/LEAF
Wavelength	0.8 - 0.85 μm	1.3 μm	1.55 μm	1.55 μm	1.55 μm
Fibre Attenuation	3 dB/km	1 dB/km	0.2 dB/km	0.2 dB/km	0.2 dB/km
Bit-rate/channel	45 Mb/s	2 Gb/s	10 Gb/s	2.5 - 10 Gb/s	40 - 100 Gb/s
Repeater distance	10 km	50 km	60 - 70 km	100 km	100 km

Table 1.1: Physical values throughout optical communications history. [2]

The first generation, commercially available from 1980, set the beginning of optical fibres, replacing coaxial lines which the spacing between repeaters was limited to 1 km [2]. From 1987, the second generation arise and the big new was the replacement of multi-mode fibres by single-mode fibres, less sensitive to the dispersion effects. Third generation's main achievement was the wavelength migration to 1.55 μm to transmit optical signals, for which the fibre loss has its minimum, i.e. 0.2 dB/km [13]. This wavelength value has been used up to the modern times. On the other hand, this wavelength order led to the usage of DSF (*dispersion-shifted fibre*), in order to minimize the dispersion. However, the usage of DSF was abandoned because it did not support WDM (*wavelength-division multiplexing*) transmission systems due to high nonlinear interaction (mainly four-wave mixing) between the optical channels. The third generation was available on the market from 1990. Later in this decade, the fourth generation came up and set the appearance of optical amplifiers namely EDFA (*Erbium doped fibre amplifier*) that reduced the need of signal regeneration [14], sharply increasing the spacing between repeaters. Adding this new to the use of DCF (*dispersion-compensating fibre*), the WDM systems became feasible since it was possible to control accumulated dispersion

and nonlinear interaction between channels, simultaneously [15]. The transmission was performed on up to 128 channels. Finally, fifth generation appeared on the market in the early 00s, introducing DWDM systems, as transmission was supported on 250 channels. By this time, the starkest limitation was over PMD and nonlinear effects.

The revival of coherent optical communications research was prompted by the modulation/demodulation experiment featuring optical in-phase (I) and quadrature (Q) modulation and optical delay detection [16]. On the other hand, polarization sensitivity was a serious disadvantage of conventional coherent receivers, but it was promptly overcome by introducing polarization diversity techniques [5]. Next stage of the revival of coherent technologies had to do with high-speed digital processing [12]. The high-speed digital integrated circuits offered the possibility of treating the electrical signal in a DSP core and retrieving the I and Q components of the complex amplitude of the optical carrier in a very stable manner. While an OPLL that locked LO phase to the signal phase was difficult to achieve, DSP circuits were increasingly faster and provided simple and efficient means of estimating the carrier phase [5]. Therefore, programmable devices started to be used for digital compensation of the optical signal, turning the coherent detection profitable and less complex.

As any long distance communication system needs to modulate a carrier signal to transmit information, optical communication systems also modulate a high-frequency carrier signal, which is particularly optical. Basically, in an optical transmission system, the binary signal which contains the information must be carried by a wave with an optical wavelength. The way as the optical carrier is modulated can be classified as direct modulation (figure 1.1a) or external modulation (figure 1.1b). Proceeding to direct modulation, the optical source (typically a laser) is modulated inside of its cavity. It consists of turning the laser on and off with an electrical drive current, yielding the "chirp" effect, which leads to a spectral linewidth enlargement. The "chirp" phenomenon is defined by a slightly shift in wavelength caused every time the laser is turned on. In the case of external modulation, the process is accomplished outside of the laser cavity, and it allows to eliminate the "chirp".

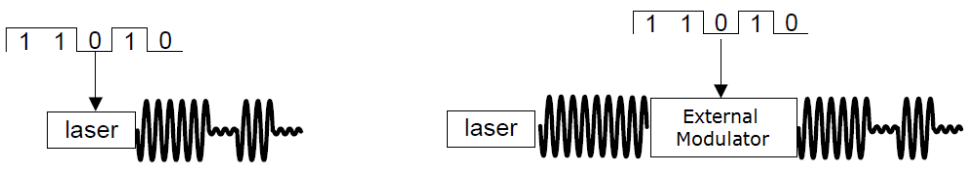

(a) Direct (b) External

Figure 1.1: OOK direct and external modulations of the laser. [17]

The modulation process can be done through different modulation formats. According to the way the signal information is modulated in the optical carrier wave, those digital modulation formats can be classified in four groups: intensity or amplitude modulation (ASK - *amplitude-shift keying*); phase modulation (PSK - *phase-shift keying*); frequency modulation (FSK - *frequency-shift keying*); polarization modulation (PolSK - *polarization-shift keying*).

FSK is rarely used in optical communication systems [18]. Due to the shape of the optical carrier, the binary ASK can also have the OOK (*on-off keying*) designation, or simply intensity modulation. There are two possible versions for the use of OOK format, in terms of pulse format: optical pulse occupying the whole bit period (NRZ - *nonreturn-to-zero*), and optical pulse occupying only a fraction of the bit period (RZ - *return-to-zero*). The ASK, as a multi-level format (M-ASK), codes M symbols for M different amplitudes. M-ASK did not prove to be profitable since the distance between symbols is smaller and it does not compensate for the higher spectral efficiency achieved by the encoding of multiple bits in one symbol. The PSK bases on the optical carrier phase modulation, keeping the amplitude as constant. PolSK can be used combined with both ASK and PSK because it allows maximizing the amount of information encoding. This takes to a higher spectral efficiency [19], which is the information rate that is possible to transmit in a certain bandwidth and it is measured in $bit/s/Hz$. However, ASK and PSK modulation formats are limited in terms of spectral efficiency and robustness to signal distortions. There was the need of using most advanced modulation formats such as QPSK.

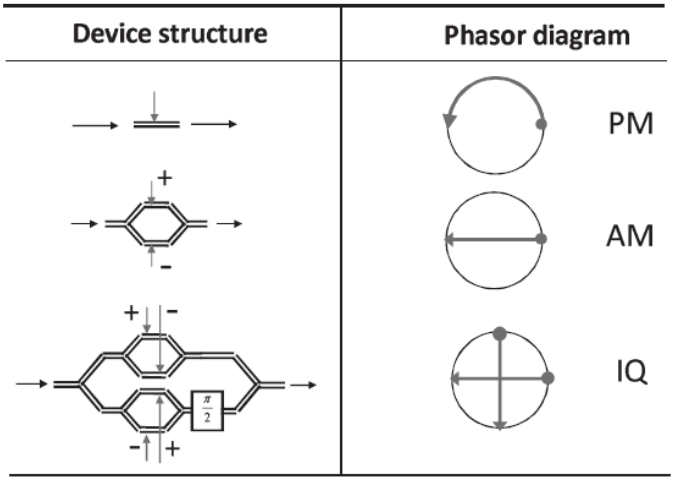

Figure 1.2: Device structure and phasor diagram of three different modulation formats. [5]

Optical PM (*phase modulation*) is simply achieved by a phase modulator, but for achieve optical AM (*amplitude modulation*), it is required the use of two phase modulators in an MZ (*Mach-Zehnder*) configuration, which is driven in a push-pull mode of operation [20]. Optical

IQ modulation, on the other hand, can be realized with MZ-type push-pull modulators in parallel, between which a $\pi/2$-phase shift is given [21]. Figure 1.2 compares phase, amplitude, and IQ modulations, in terms of device structure and phasor diagram.

While the spectral efficiency of binary modulation formats is limited to 1 $bit/s/Hz$ per polarization, which is called the Nyquist limit, multi-level modulation formats, i.e., with M bits of information per symbol, can achieve up to spectral efficiency of M $bit/s/Hz$ per polarization [5]. Although optical delay detection has been employed to demodulate the QPSK signal (M=2), a further increase in multiplicity was hardly achieved with such a format. As example, figure 1.3 shows 4 different modulation formats, transmitting 1 bit, 2 bits, 3 bits, and 4 bits per symbol [5].

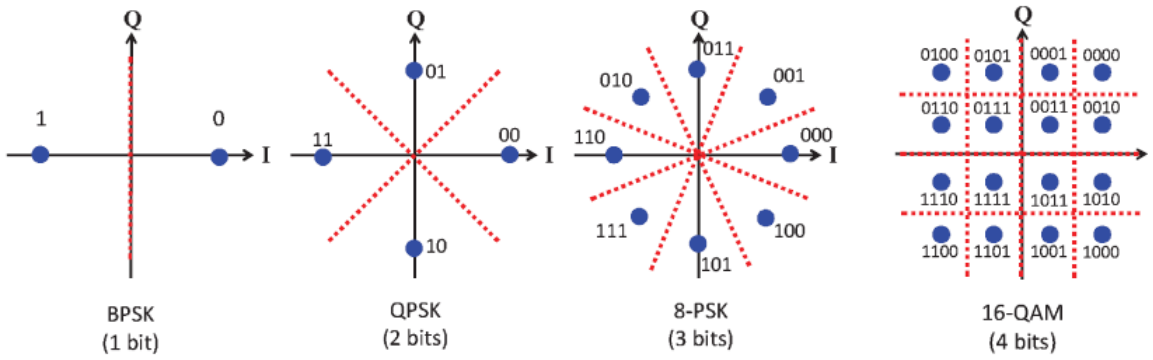

Figure 1.3: Four constellation maps regarding phase modulation. [5]

Also known by 4-QAM, the QPSK modulation format is the leading candidate for high speed fibre networks due to its high performance, spectral efficiency and its relatively low complexity of implementation [22]. It presents a four-point constellation on the complex plane. Using such a modulation format, one symbol carries two bits and that enables doubling the bit rate while keeping the symbol rate or, on the other hand, keep the bit rate with the halved spectral width [5]. This means the bandwidth of a QPSK signal is half of the bandwidth of an ASK/PSK signal (which equals the double of the baseband if the pulse format is NRZ). So the spectral efficiency of a QPSK is twice greater than a simple ASK/PSK.

QPSK is nothing but a two-dimensional modulation format spanned by the in-phase and quadrature components of the optical field. The polarization states are considered two independent channels where the modulation format can be transmitted to double the throughput [23]. QPSK is also considered a linear modulation format since the resulting modulated signal is a linear combination of the symbols being sent. I and Q together offer two degrees of freedom over which to distribute the symbol alphabet. QPSK distributes four points on the unit circle, equidistant from each other [24].

Since coherent systems allow access to the full optical field, they offers the possibility to use more spectrally efficient and/or more sensitive formats, such as PM-QPSK (*polarization-multiplexed quadrature phase-shift keying*), which is a QPSK version. Good sensitivity and low complexity in terms of hardware and receiver DSP led to consider this modulation format as the most studied one on coherent fibre optical communication systems [25]. PM-QPSK presents independent constellations for each polarization state. Note that a PM-QPSK signal is obtained by a system based on two IQ-modulators, one for each polarization, driven by binary drive signals with a typical voltage swing of $2V_\pi$. The two optical signals are combined with orthogonal polarization states using a PBC (*polarization beam combiner*) [23]. However, this dissertation refers most of the time to the simple QPSK modulation format since it is considered only one polarization as example.

Additionally to the advanced modulation formats, the coherent detection came up to replace the direct detection, in order to enhance the usage of post-DSP in optical reception. Despite the low complexity and low cost of IM/DD systems, these ones only allow detecting the information modulated in amplitude. Direct detection is incompatible with advanced modulated formats and it limits the sensibility itself, beyond that it does not encourage the spectral optimization of the optical system. This turns the DSP unsuitable and it demands the usage of an alternative and more efficient detection type: optical coherent detection.

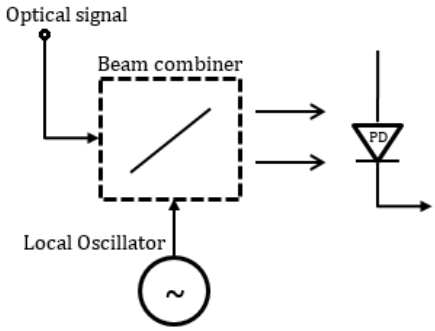

Figure 1.4: Overall coherent detector schematic.

The main characteristic of the coherent detection is the equality between the polarization of the incoming signal and the LO [4]. The fields of the signal and LO are of constant amplitude over the surface of the detector. A coherent detector enables the detection of the information modulated also in phase [19]. This way, as well as compatible with advanced modulation formats, it turns possible the post-DSP of the detected signal, which the performance takes to a more robust optical system. Both the amplitude and the relative phase

information between the conjugate signals can be extracted via differential detection and DSP. Moreover, in a coherent receiver system, the preservation of the optical phase can be used to cost effectively compensate optical transmission impairments in the electrical domain.

Beyond the maximization of spectral efficiency and power efficiency, the coherent detection presents other advantages such as higher receiver sensitivity, lower channel crosstalk and still ensures a more secure communication.

The receiver front-end can present two different configurations, according to the down-conversion process: heterodyne shown in figure 1.5a, and homodyne shown in figure 1.5b.

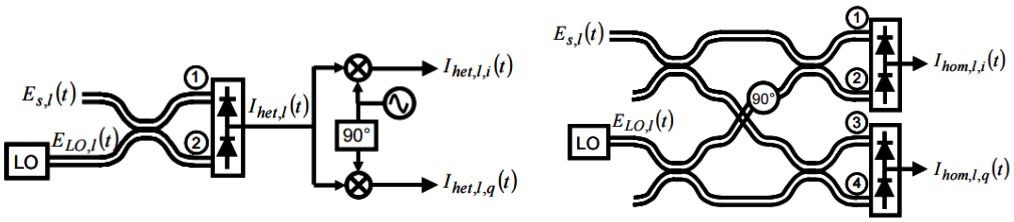

(a) heterodyne design [19] (b) homodyne design [19]

Figure 1.5: Downconverter employing both designs, regarding a single polarization.

Basically, the two configurations above define the way as the downconversion from optical passband to electrical baseband is achieved. For the heterodyne downconverter, the LO and transmitter lasers differ by an intermediate frequency, and an electrical LO is used to down-convert that intermediate frequency signal to baseband. In the homodyne downconverter, the frequency of the LO laser is tuned to that of the transmitter laser so the photodetector output is at baseband [19].

The adopted downconversion for the current QPSK receiver corresponds to the homodyne configuration, once it is the one used in the lab of Optics. A major advantage of the homodyne front-end over a heterodyne one is the fact of each photodetector needs less bandwidth than a photodetector placed in a heterodyne front-end. On the other hand, the homodyne one requires twice the number of balanced photodetectors.

With the data rates increase as well as fibre lengths increase, limitations due to dispersion had to be avoided somehow. Hereupon, to get around the dispersion problems, it was proceeded to optical compensation which in coherent transmission systems is evolved into digital terms. Digital coherent receivers allow equalization of fibre dispersion in the electrical domain [3] and have become the most promising alternative approach to DCFs [26].

Digital post-processing allowed the usage of free-running LOs where the phase-tracking is done in the digital domain rather than with complex implementation in hardware such

as phase-locked loop circuits [23]. So DSP consists of a set of algorithms aiming the digital equalization of the incoming signal in the optical coherent receiver. Those algorithms must be adapted to the used modulation format, because the impairments they are supposed to compensate depends, mostly, on the imperfections of the modulator, located in the transmitter, and demodulator, located in the receiver. On QPSK modulation case, the transmitted optical signal can be distorted by imperfections such as non-ideal bias for the I and Q signals as well as the 90°-phase shift in the IQ-modulator, imperfect splitting ratio of the optical signal, different amplitude of the RF driving signals or different gain of the drive-amplifiers as well as non-ideal polarization splitting can distort the signal. On the receiver side, the impairments are mainly due to 90° hybrid imperfections and differing responsivities of the photodetectors.

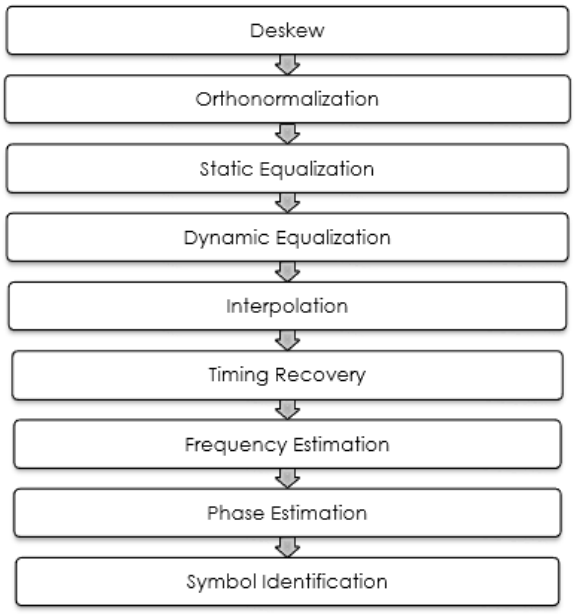

Figure 1.6: DSP stages in an optical coherent receiver. [27]

The first two stages of digital post-processing aim to compensate for eventual impairments of the optical demodulator. Deskew is the stage which compensates for the impairments caused by time delays and orthonormalization solves phase and amplitude impairments. Both occur as a result of the two branches of optical hybrid outputs.

The third and fourth stages consist of static and dynamic equalizations for deterministic and stochastic effects, respectively. The static equalization compensates for the CD linear effects, which can be eventually non-linear. The dynamic equalization is required by PMD due to its random behaviour, i.e. resulting in non-linear effects.

There is an unavoidable time deviation of the optimum sampling instant due to ADC defects. This behaviour demands the implementation of clock recovering functions that involve interpolation stages and re-sampling (designated by timing recovery).

Also, the frequency and phase suffer deviations due to the free operation of the LO in coherent receivers. Finally, the digital post-processing ends with symbol identification and decoding [4].

As it was said so far, DSP is responsible for a great progress in coherent systems, once it allows mitigating the signal distortions. This progress increased the efficiency of the optical transmission systems, enabling transmission with higher bit-rates and higher ranges. The stages of DSP in coherent receivers involve the tasks of clock recovery, carrier recovery, and symbol decoding, which are achievable using several digital techniques, including equalization. The digital equalization is nowadays implemented by software, under algorithm forms, performing linear or adaptive filtering of the digital signal, by resorting to FIR (*finite impulse response*) [28] and IIR (*infinite impulse response*) [29] filters. This means the equalization process can be static or dynamic, according to the impairments that are supposed to compensate. The impairments sources can be classified as linear (e.g. CD - *chromatic dispersion*) or nonlinear (e.g. PMD - *polarization mode dispersion*). However, this chapter is focused exclusively on the digital CD equalization, that means the static strand.

Dispersion can be compensated without penalty either in the time or frequency domain [3], but the computational complexity of an FIR filter convolution surpasses a frequency domain approach already for a small number of taps [30] [31]. In a frequency-based approach, the signal has to be transformed by an FFT (*fast Fourier transform*) and multiplied by the inverse of the transfer function of the dispersive channel in the FDE (*frequency-domain equalizer*). Algorithms like LMS (*least mean square*) [32] or the CMA (*constant-modulus algorithm*) [33] can be adapted to the frequency domain as well.

The requirements of the CD compensation rely on using narrow spectral width optical sources, i.e. high precision lasers, using external modulation and NRZ [34]. The NRZ pulse format is used rather than, for instance, the 50% RZ because NRZ takes to obtain a higher dispersion length. It still allows decreasing the spectral linewidth and that results in a lower dispersion effect.

Chapter 2

PM-QPSK Optical Transmission Systems

The second Chapter aims to describe an end-to-end PM-QPSK optical transmission system. Section 2.1 is dedicated to the transmitter, where each block is described in the following Subsections, in order to understand the task of each one within the transmission circuit. Beyond the building blocks description, there are presented some results obtained from a simulation environment, which help to understand how the transmitter behaves in reality. Section 2.2 refers to the optical channel furthering the relevant issues for the later simulations in the Chapters 3 and 4. Section 2.3, similarly to the Section 2.1, describes each receptor's building block, just does not contain any simulation results.

2.1 Transmitter

This Section may contextualize the research work, introducing the first stage of an overall optical transmission system: the transmitter. In order to approximately represent such a circuit, there were considered several blocks. Since this optical signal is associated to the modulation format QPSK, that means the existence of the two components I and Q which are processed separately, reason why the block diagram in figure 2.1 presents two branches.

A partial simulation environment of the QPSK transmission system was taken at this point, in order to get some simulation results of each building block. This simulation environment, implemented by C++ code, has been developed among the students from Optical Communications group, using the web hosting repository GitHub®. The idea was to adjust the code in order to create an environment that might serve as a replication of the physical transmitter set up in the lab of Optics in *Instituto de Telecomunicações*. Moreover, it allows to run very large binary sequences (up to $2^{26} - 1$ bits) fast.

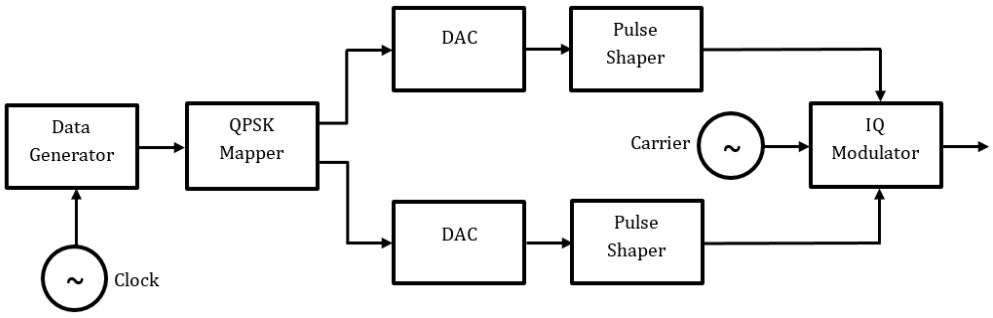

Figure 2.1: Block diagram of an overall QPSK transmitter.

Once the optical channel and the QPSK reception system were not developed yet, within the mentioned simulation environment, these parts were just simulated using MATLAB® instead, whose results are presented in the Chapters 3 and 4. Otherwise, these parts of the QPSK transmission systems would take a lot of time to be developed and then simulated.

Below, there are presented the user's adjustable settings for each block of the QPSK transmitter, which are explained in detail in the further Subsections. Beyond containing the theoretical explanation of each block, each Subsection is followed by the respective results obtained from the transmitter's simulation. Those results are based on a simulation settling the presented values, which are simply illustrative. There were also made some code adjustments, with more emphasis on PRBS generator, i.e. first transmitter's block (in 2.1.1). It is important to add that the blocks correspond to "classes", in programming terms.

Binary Source		***DAC***		***Pulse Shaper***	
Mode	'PseudoRandom'	Samples per symbol	5	Rolloff factor	0.09
Pattern length	5			Number of taps	24
Bit stream	'00101'				
Bit period	1/50E9				
Number of bits	10000				

Table 2.1: Settings and respective chosen values for simulating.

The proposed values in the table 2.1 regard a PRBS generator with the initial sequence '00101'. It generates full sequences of 2^5-1 bits, up to 10000 bits. The bit rate is 25 Gb/s and since this transmission system regards a QPSK format, each 2 bits correspond to one symbol, then the symbol rate is 12.5 Gb/s. The number samples per symbol is set to 5, meaning a sample rate of 5 times the symbol rate, so 62.5 Gb/s[1]. Finally, the rolloff factor for the pulse shaper is 0.09 and its number of taps is 24. The block diagram in figure 2.2 represents the code structure of the simulation environment for the QPSK transmitter.

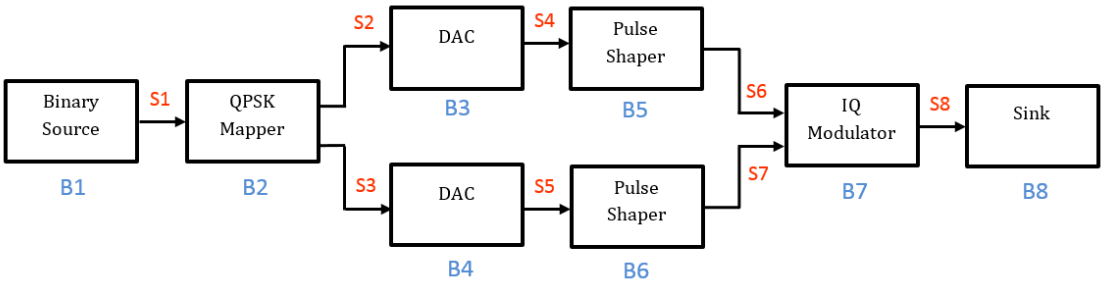

Figure 2.2: Block diagram of the transmitter implemented in C++, with signals and blocks represented numerically.

2.1.1 Data Generator

The data generator transmits the optical information signal according to a cycle set by an external clock signal. The data generator corresponds then to a PRBS (*pseudo-random binary sequence*) which consists of a deterministic binary sequence repeated infinitely, the reason why is pseudo-random. This is the way as it is possible to recreate a real data sequence, which is random in fact. A random binary sequence is a statistically independent sequence of 0's and 1's, each occurring with a probability of 50% [35].

One of the upgrades in the C++ transmitter consisted of adding a feature that allows the user to make the bitstream setting, in other words, make the manual initialization for the PRBS. That feature was added to the class *Binary Source* (block *B1* in figure 2.2). Obviously, the introduction of such feature implied a validation and error functions, both presented in Appendix A. The other upgrade consisted of improving and ensure the proper functioning of the PRBS generator.

[1]These values of bit and sample rates are the proper ones to simulate a sequence in the lab, due to AWG's bandwidth constraints.

Pseudo-Random Test Patterns

In order to validate the algorithm which simulates the PRBS generator, there were made several tests over it, such as sequences validation and periodicity test.

A pseudo-random binary sequence is supposed to be a periodic binary sequence with an autocorrelation function that resembles the autocorrelation function of a random binary sequence. This PRBS is generated by an LFSR (*linear feedback shift register*), represented on figure 2.3), whose arrangement consists of binary storage elements and feedback logic. Binary sequences are shifted through the shift register in response to clock pulses. The contents are logically combined by an *XOR*, in this case, to produce the input to the first stage, which means the initial contents and feedback logic determine the successive contents of the shift register [35].

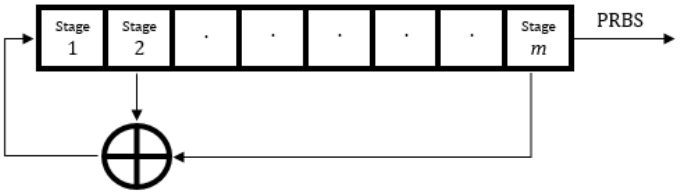

Figure 2.3: M-stage linear feedback shift register for generating PRBS.

For simulation effects, the considered initial contents consisted on a sequence with at least one state set to '1'. If an LFSR contains all zeros at any time, it will be stuck in that state forever. Since there are exactly $2^m - 1$ non-zero states, the maximum period cannot exceed $2^m - 1$, as well [35]. Moreover, the number of distinct states in an m-state shift register is 2^m, so the sequence of states and the output sequences must be periodic, for a period of at most 2^m. This characteristic had to be verified through a function developed in MATLAB® that is presented in Appendix B.

The following table 2.2 is the result of various simulations in order to find the respective feedback polynomials to each sequence pattern length, which equals the LFSR length, or the number of stages. The polynomial coefficients were taken from [35] and [36].

Right after, it is presented an exampling table 2.3 with some binary sequences generated by applying the previous polynomials. The table includes the pattern length, m, the period length of the binary sequence, $2^m - 1$, and also the data length, $2^m + m - 2$, which equals the period length plus the necessary margin to ensure the validation of the last sequence values.

m	Feedback polynomial	Ref.	m	Feedback polynomial	Ref.
1	[1]	[35]	14	[2,12,13,14]	[36]
2	[1,2]	[35]	15	[1,15]	[36]
3	[1,3]	[35]	16	[2,3,5,16]	[36]
4	[1,4]	[35]	17	[14,17]	[36]
5	[1,2,4,5]	[35]	18	[1,2,5,18]	[36]
6	[2,3,5,6]	[35]	19	[1,2,5,19]	[36]
7	[1,7]	[36]	20	[8,9,17,20]	[37]
8	[2,3,4,8]	[35]	21	[19,21]	[36]
9	[3,4,6,9]	[35]	22	[1,22]	[36]
10	[3,10]	[35]	23	[5,23]	[36]
11	[2,5,8,11]	[35]	24	[1,3,4,24]	[36]
12	[1,4,6,12]	[35]	25	[3,25]	[36]
13	[1,3,4,13]	[35]	26	[8,24,25,26]	[37]

Table 2.2: Feedback polynomials for each shift register stage.

m	$2^m - 1$	$2^m + m - 2$	Binary sequence
1	1	1	1
2	3	4	0110
3	7	9	101001110
4	15	18	000111101011001000
5	31	35	00101111101100111000011010100100010
6	63	68	10000111000001011111100101010001100...
⋮	⋮	⋮	⋮
26	67108863	67108888	...

Table 2.3: Binary sequences generated for different pattern lengths, from 1 to 26.

Finally, it was proceeded to the implementation of a MATLAB function, also presented in Appendix B, which validates a binary sequence of any length. The table 2.4 exemplifies the validation process, presenting all the possible values inside a binary sequence generated with a certain pattern length. In this case, pattern length equals 5, whose feedback polynomial is $(x^5 + x^4 + x^2 + x^1 + 1)$ according to table 2.2.

State	Binary value	Decimal value
1	00101	5
2	01011	11
3	10111	23
4	01111	15
5	11111	31
6	11110	30
7	11101	29
8	11011	27
9	10110	22
10	01100	12
11	11001	25
12	10011	19
13	00111	7
14	01110	14
15	11100	28
16	11000	24
17	10000	16
18	00001	1
19	00011	3
20	00110	6
21	01101	13
22	11010	26
23	10101	21
24	01010	10
25	10100	20
26	01001	9
27	10010	18
28	00100	4
29	01000	8
30	10001	17
31	00010	2

Table 2.4: Validation for generated sequence with pattern length of 5.

In order to corroborate the validation MATLAB function present in Appendix B and the chosen feedback polynomials, it was made the same validation for the same pattern length values but this time using the PN Sequence Generator block in Simulink®. This block is a pseudo-noise generator that belongs to Communications System Toolbox™ of MATLAB®. Figure 2.4 shows an example of the settings window for a pattern length of 5. The whole transmission system was also simulated in Simulink® and its block diagram can be consulted in the figure 2.5.

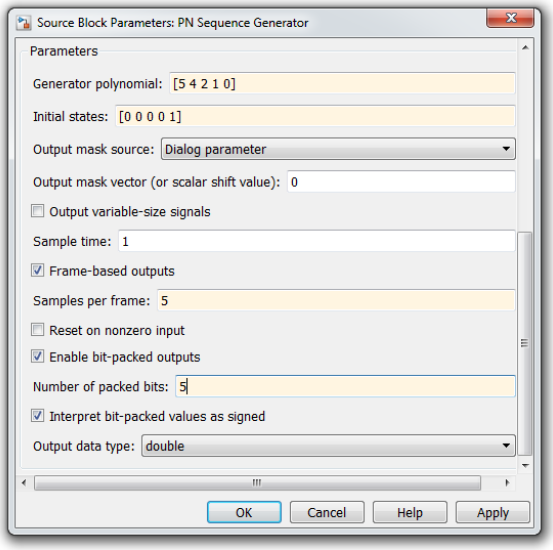

Figure 2.4: Settings window of the PN Sequence Generator block in Simulink®.

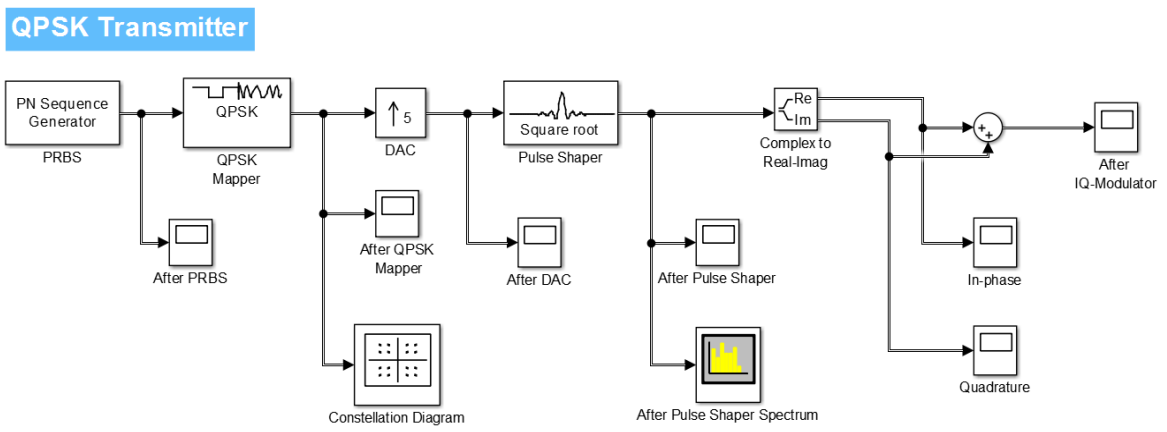

Figure 2.5: Block diagram of a QPSK transmitter in Simulink®.

At last, figure 2.6 shows a time domain graph[2] of the data generator output signal (*S1* in figure 2.2) resulting from a simulation where it is considered a pattern length of 5 as well. The logical values observed in the graph corresponds to the binary sequence in table 2.3, for the same pattern length. The sequence period is 0.62 ns, once the bit rate was set to 50 Gb/s, meaning a bit period of 20 ps:

$$(2^m - 1)bits = 31bits, \qquad with \quad m = 5, \tag{2.1}$$

$$T_{seq} = T_{bit} \times 31bits = 0.62ns, \qquad with \quad T_{bit} = 20ps. \tag{2.2}$$

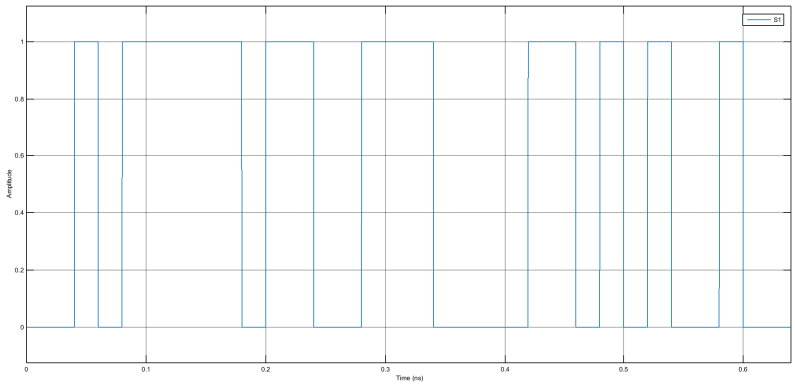

Figure 2.6: PRBS output signal in time domain.

2.1.2 *M*-QAM Mapper

In this specific case, the M-QAM mapper is a QPSK mapper as it is shown in figure 2.1. The binary sequence is grouped in sets of two bits which will correspond to one of the four symbols placed in the constellation map, where each one has $2D$ coordinates associated. This block represents the mapping process (block *B2* in figure 2.2), digitally performed by mapping the binary sequence from data generator using a QPSK constellation map, previously defined: Gray-scaled or binary-scaled. It was chosen the Gray encoding for the current QPSK mapper, since it allows the minimization of bit errors by causing adjacent symbols to only be one bit off from their neighbours. In case of binary encoding, the adjacent symbols on the positive real plan of the constellation map (figure 2.7a) differ by two bits unlike the Gray-coded signal constellation (figure 2.7b), where each symbol differs by only one bit from its direct neighbours, which leads to a better BER (*bit error rate*) performance.

[2]This graph and the following ones, regarding each signal of the QPSK transmitter, were obtained with the program tool Visualizer™, developed in MATLAB®, that works as a virtual oscilloscope.

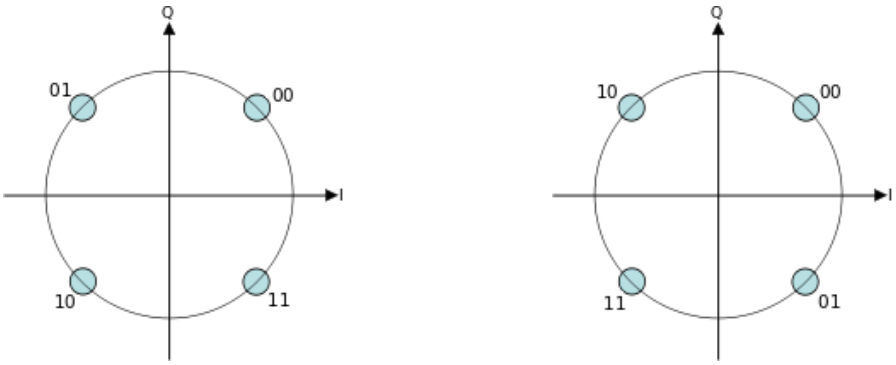

(a) Binary-coded (b) Gray-coded

Figure 2.7: Constellations of signals coded by different scales.

In the figures 2.8a and 2.8b, it is possible to observe the mapping result from the constellation mentioned above through figure 2.7b. The mapping process leads to having two signals, which the period corresponds to the symbol period and it equals the double of the bit period, so 40 *ps* because each symbol is composed of two bits.

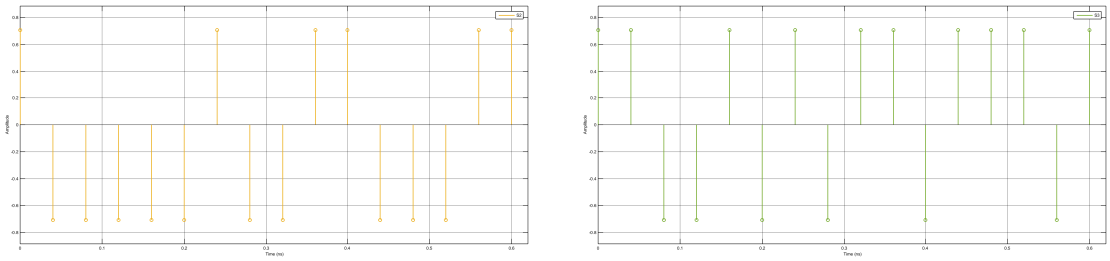

(a) In-phase (b) Quadrature

Figure 2.8: *Discrete time - discrete amplitude* real signal outputted by M-QAM mapper.

In-phase	+	-	-	-	-	-	+	-	-	+	+	-	-	-	+	+
Quadrature	+	+	-	-	+	-	+	-	+	+	-	+	+	+	-	+
Symbol	00	10	11	11	10	11	00	11	10	00	01	10	10	10	01	00

Table 2.5: Coordinates signs and respective symbols.

Table 2.5 presents the coordinates sign (in-phase and quadrature), read from the figures 2.8, as well as the respective symbols. Following the order of the obtained symbol sequence, in the last row of table 2.5, it is possible to conclude that it corresponds to the binary sequence of table 2.3, once again. The matching made in table 2.5 faces the constellation implemented, whose diagram is described in detail by figure 2.9 and by table 2.6.

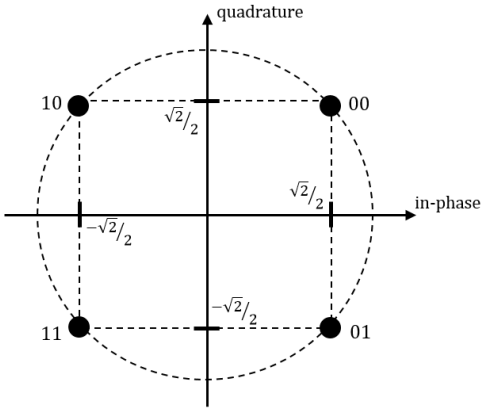

Figure 2.9: QPSK constellation diagram.

Coordinates (*I*, *Q*)	**Symbol**
$\left(\frac{\sqrt{2}}{2}, \frac{\sqrt{2}}{2}\right)$	00
$\left(-\frac{\sqrt{2}}{2}, \frac{\sqrt{2}}{2}\right)$	10
$\left(-\frac{\sqrt{2}}{2}, -\frac{\sqrt{2}}{2}\right)$	11
$\left(\frac{\sqrt{2}}{2}, -\frac{\sqrt{2}}{2}\right)$	01

Table 2.6: Coordinates and respective symbols.

2.1.3 Digital-to-Analog Converter

DAC block regards the conversion of the signal from the digital domain to the analog domain over time, i.e. the inverse operation for oversampling. In this stage of the transmitter system, there are two branches because of the mapping, so there are two DAC blocks (*B3* and *B4* in fig. 2.2): one for the in-phase branch, another one for quadrature branch. In fact, these blocks implemented in C++ do not turn the discrete signal in a continuous one, since they are digitally processed. They make a signal upsampling, by adding '0's, in order to simulate a continuous signal.

The figures 2.10 present the DAC result over the digital in-phase and quadrature signals, which is a set of Dirac pulses. Comparing with the figures 2.8, it is possible to see that the amplitude values over symbol period multiple instants are exactly the same. The only difference is about the increase of the number of samples per symbol. The value of this number is adjustable by the user and, in this case, was set to 16.

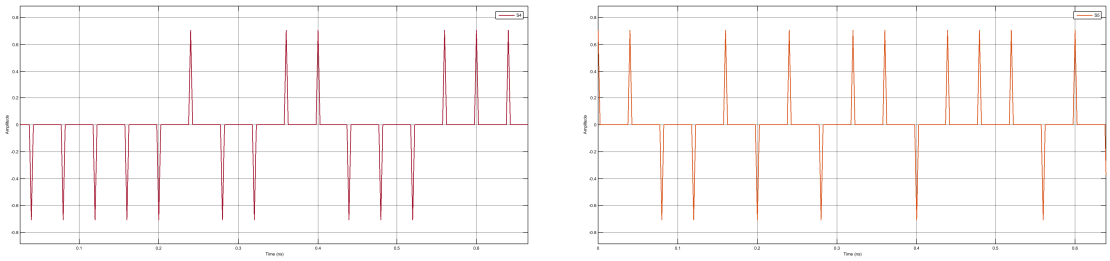

(a) In-phase (b) Quadrature

Figure 2.10: *Continuous time - discrete amplitude* real signal outputted by DAC.

2.1.4 Pulse Shaper

This block shapes the DAC output signal in amplitude domain, then it goes something like the inverse operation for quantization. The symbol pulse shaping process is performed in order to obtain a zero-ISI characteristic and a filter which maintains this characteristic is often called a "Nyquist filter". The pulse shaper aims to solve two conflicting requirements: the demand for high data rates, and the need for narrower bandwidth, consequently resulting in the need of more transmitting channels in the optical link with less noise. One possible solution is to use an ideal LPF (*low-pass filter*), which corresponds to a rectangular shape in the frequency domain. But this filter is physically unrealisable and difficult to approximate since it requires extreme precise synchronization and jitter might be detrimental in the system. This led to an alternative solution: the raised cosine filter. This filter type is physically feasible hence it is the one used in the majority of real communication systems and it is based on a Nyquist principle. Such principle states that if the frequency characteristic has odd symmetry at the cutoff frequency, the impulse response will have zeros at uniformly spaced intervals [38].

The following equations, taken from [38], show the difference between the previous described filters, firstly in terms of bandwidth, and secondly in terms of pulse function:

$$B = f_c = \frac{1}{2T}, \tag{2.3}$$

$$B = (1+\beta)\, f_c = \frac{1+\beta}{2T}, \tag{2.4}$$

$$h(t) = \frac{\sin\left(\frac{\pi t}{T}\right)}{\frac{\pi t}{T}} \quad \Longrightarrow \quad h(t) = sinc\left(\frac{\pi t}{T}\right), \tag{2.5}$$

$$h(t) = \frac{\sin\left(\frac{\pi t}{T}\right)}{\frac{\pi t}{T}} \frac{\cos\left(\frac{\pi \beta t}{T}\right)}{1 - \left(\frac{4\beta^2 t^2}{T^2}\right)} \quad , \tag{2.6}$$

where T is the sampling time, β is the rolloff factor (further explained) and f_c is the cutoff frequency. The equation 2.3 regards the baseband transmission bandwidth using an ideal LPF that equals the Nyquist band ($B = 1/2T$) whereas the equation 2.4, regarding the baseband bandwidth using a raised cosine filter, the Nyquist bandwidth times $(1 + \beta)$. Therefore, the raised cosine filter is more bandwidth efficient than rectangular shaping [38]. Referring the pulse functions below, the equation 2.5 is a *sinc* function and it yields a rectangular pulse shape whereas the pulse represented by equation 2.6 presents a first term with the previous *sinc*, that ensures the roots as like ideal LPF, and a second term which decays in time, that leads to a reduction of the jitter impact [38].

The raised cosine filter has the shape of the filter transition band, in frequency domain, which follows a half-cycle of a raised cosine shape. A useful characteristic of this filter response is that it is infinitely adjustable and represents a family of responses [39]. The adjustment characteristic is the EBW (*excess bandwidth*), or often referred as "rolloff factor". This characteristic describes how far the transition band extends as a percent of the distance to the cosine inflection point in the centre of the transition band. The rolloff factor selection allows to trade off various system design considerations [39]. Lower EBW gives narrower bandwidth. However, the side lobes of its shape increase so attenuation in stop band is reduced [38]. Beyond the occupied bandwidth increase with EBW, there are other tradeoffs associated with the choice of this parameter. A low EBW means a high PAPR (*peak-to-average power ratio*) as well as the length of the impulse response necessary to be computed in digital processing without losing significant performance. On the other hand, a low percentage of EBW may be advantageous in communications systems that need closely spaced carriers in order to maximize the number of channels in a band. The PAPR decrease with EBW increase is observable through an eye diagram: the higher the EBW, more stretched and open is the eye diagram, i.e. the eye diagram opens up. This results on a system less sensitive to jitter in the symbol recovery clock since a deviation from the zero-ISI sampling point will generate a smaller potential error than it would with a low EBW pulse [39]. In a case of no bandwidth restrictions, it would be easier on the receiver if it would be used a high EBW. However, in terms of bandwidth efficiency, EBW should be lower [38].

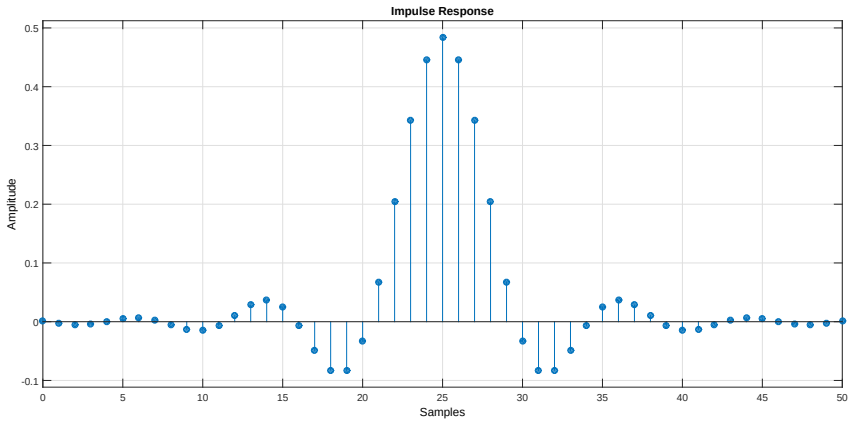

Figure 2.11: Illustrative impulse response of a raised cosine filter, with rolloff factor = 0.3.

Beyond rolloff factor, another adjustable pulse shaper's setting in the developed QPSK transmitter is the number of taps. This parameter regards the amount of memory required to implement the filter as well as the number of calculations required. More taps mean more stop-bandwidth attenuation, less ripple, and a narrower filter. The example of figure 2.11 regards an ideal raised cosine filter and that means an infinite number of taps. In the C++ transmitter, the pulse shaping blocks implement raised cosine filters, corresponding to *B5* and *B6* in figure 2.2, whose rolloff factor was set to 0.09 and whose number of taps was set to 24.

In the figures 2.12 and 2.13, regarding the in-phase and quadrature branches respectively, it is possible to observe the pulse shaper's output in the time domain as well as its eye diagram.

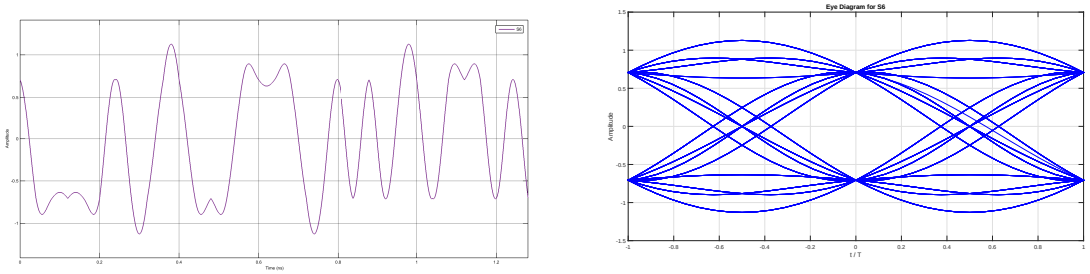

(a) Signal in time domain

(b) Respective eye diagram

Figure 2.12: *Continuous time - continuous amplitude* real signal outputted by the in-phase branch of pulse shaper.

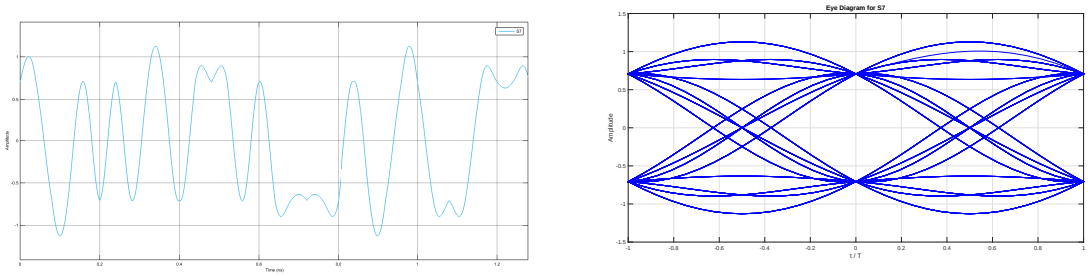

(a) Signal in time domain (b) Respective eye diagram

Figure 2.13: *Continuous time - continuous amplitude* real signal outputted by quadrature branch of pulse shaper.

The time domain graphics 2.12a (signal *S6*) and 2.13a (signal *S7*) show the shaping result on the *S4* and *S5* signals, that only had two possible amplitudes. As it was said before, pulse shaper's rolloff factor was set to 0.09 and number of taps was set to 24. Considering these values, the yielded eye diagrams 2.12b and 2.13b present a proper layout, with zero-ISI.

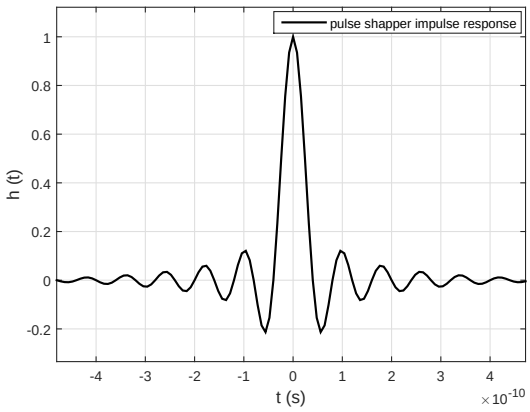

Figure 2.14: Impulse response of pulse shaper.

The figure 2.14, also obtained with the Visualizer™, represents the impulse response of the pulse shaper. Observing the figure it is possible to reach two relevant facts. In the first figure, the central lobe corresponds to a time band which equals twice the duration of the transmission of one sequence, i.e. $2{\times}0.62\ ns$.

2.1.5 IQ-Modulator

This last stage of the transmission system is responsible for turning the electrical into an optical one. IQ modulation can be realized with MZ-type push-pull modulators in parallel, between which a $\pi/2$-phase is given [21], shown by figure 2.15. The two input baseband

signals are orthogonal and therefore transmitted simultaneously and fully recovered at the receiver side. This sort of modulation fits in the external modulation, already explained above.

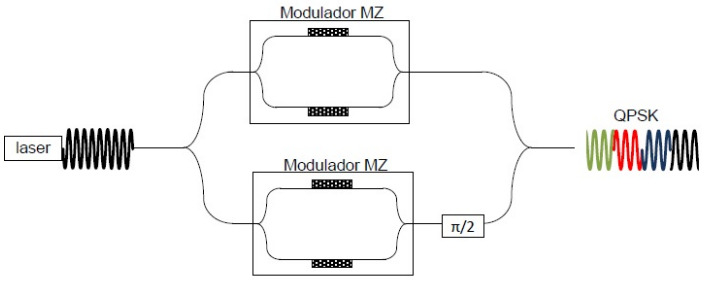

Figure 2.15: IQ-modulator schematic. [17]

The equations below, associated to figure 2.16, give an analytical view of this modulation type, which is valid for radio-frequencies:

$$\mathrm{i}_t(t) = \mathrm{i}(t)\cos\left(2\pi f_o t\right), \tag{2.7}$$

$$q_t(t) = q(t)\cos\left(2\pi f_o t + \frac{\pi}{2}\right) = q(t)\sin\left(2\pi f_o t\right), \tag{2.8}$$

$$y_t(t) = \sqrt{\mathrm{i}^2(t) + q^2(t)}\cos\left(2\pi f_o t + \theta(t)\right), \quad with - \pi < \theta < \pi, \tag{2.9}$$

where $\mathrm{i}(t)$ and $q(t)$ are the I and Q baseband signals, f_o is the optical carrier, $\mathrm{i}_t(t)$ and $q_t(t)$ are I and Q transmitted signals, $y_t(t)$ is the sum of the two transmitted signals thereupon forwarded through the fibre, and finally $\theta(t) = \tan^{-1}\frac{q(t)}{\mathrm{i}(t)}$.

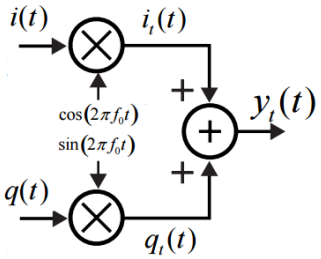

Figure 2.16: Analytical schematic of the IQ-modulator.

The QPSK modulated signal is obtained from the binary amplitude modulation of an optical carrier by the in-phase (I channel) and quadrature (Q channel) waveforms. The optical signal, provided by an ideal laser, is divided into two branches to be phase modulated between the symbols '0' and 'π'. Then, it is added a '$\pi/2$' delay to one of the MZ-modulators output. The interference result between the modulator branches is the set of symbols $\{-\pi/4; -3\pi/4; +3\pi/4; +\pi/4\}$ [17].

For optical frequencies, the previous equations are not applicable. Therefore, the MZ modulator's transfer function (without considering insertion loss) has to be given by:

$$\frac{E_{out}(t)}{E_{in}(t)} = \frac{1}{2}\left(e^{i\varphi_1(t)} + e^{i\varphi_2(t)}\right), \tag{2.10}$$

whose the phase shifts of the upper arm, $\varphi_1(t)$, and the lower arm, $\varphi_2(t)$, are given by:

$$\varphi_1(t) = \frac{u_1(t)}{V_{\pi 1}}\pi, \quad \varphi_2(t) = \frac{u_2(t)}{V_{\pi 2}}\pi, \tag{2.11}$$

where $u_1(t)$, $u_2(t)$ are the driving signals of both arms, and $V_{\pi 1}$, $V_{\pi 2}$ are the driving voltages to obtain a phase shift of π. In a dual-drive MZ modulator, the phase modulators in both arms can be driven independently [40]. The push-pull mode means that an identical phase shift is induced in both arms, then $\varphi(t) = \varphi_1(t) = \varphi_2(t)$. If $\varphi_1(t) = -\varphi_2(t)$, whereupon $u_1(t) = -u_2(t) = u(t)/2$, it also operates in push-pull mode but obtaining a "chirp"-free amplitude modulation:

$$\frac{E_{out}(t)}{E_{in}(t)} = \cos\left(\frac{\Delta\varphi_{mz}(t)}{2}\right) = \cos\left(\frac{u(t)}{2V_\pi}\pi\right). \tag{2.12}$$

The incoming light (laser) is equally split into two arms (I and Q). In each arm, there is an MZ-modulator operating in push-pull mode. A relative phase shift of $\pi/2$ is adjusted in one arm, for instance by a phase-modulator: $u_{PM} = -\frac{V_\pi}{2}$ as driving voltage.

IQ-modulator's transfer function (neglecting any insertion loss) [40]:

$$\frac{E_{out}(t)}{E_{in}(t)} = \frac{1}{2}\cos\left(\frac{\Delta\varphi_I(t)}{2}\right) + i\frac{1}{2}\cos\left(\frac{\Delta\varphi_Q(t)}{2}\right), \tag{2.13}$$

$$\Delta\varphi_I(t) = \frac{u_I(t)}{V_\pi}\pi, \qquad \Delta\varphi_Q(t) = \frac{u_Q(t)}{V_\pi}\pi, \tag{2.14}$$

where $\Delta\varphi_I(t)$ and $\Delta\varphi_Q(t)$ correspond to the phase shifts of both arms.

Lastly, figure 2.17 presents the squared amplitude and phase of the complex signal *S8* given by $I + iQ$, i.e. *S6* for the real part and *S7* for the imaginary part.

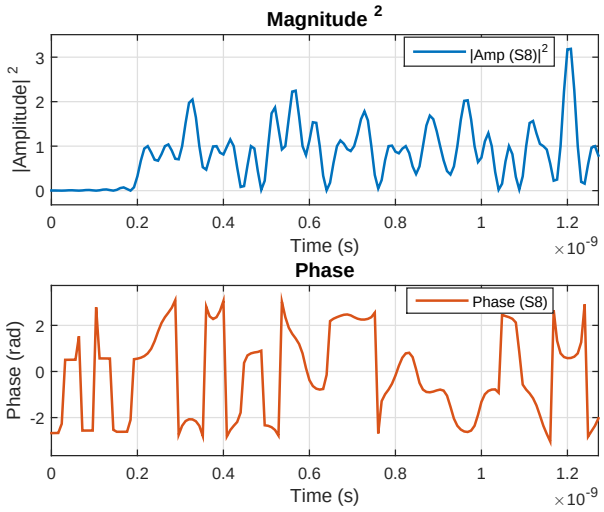

Figure 2.17: Amplitude squared and phase of the *continuous time - continuous amplitude* complex signal outputted by IQ-modulator.

2.2 Optical Channel

The communication channel may transport the signal from transmitter to receiver. The typical communication channels for transmission of the optical signals are optical fibres made of silica glass, whose principle is the total internal reflection. They allow transmitting with losses as small as 0.2 dB/km, which means an optical power reduction of only 1% after 100 km. For long-haul optical systems typically span lengths of 50-120 km are used, where the optical signal is amplified after each span.

Beyond attenuation, an important issue to consider along the optical fibres is dispersion. This phenomenon can spread significantly the optical pulses outside their allocated bit slot and, consequently, degrade the signal severely [2]. There are three dispersion types likely to happen in the optical links. They are modal, chromatic (CD) and polarization mode (PMD). It is important to make clear that this dissertation deals only with SMFs and therefore modal dispersion, which occurs only in MMFs, is not considered. The same for PMD, which is not considered. SMFs only support the fundamental mode of the fibre. The group velocity associated with that fundamental mode is frequency dependent because of chromatic dispersion. It results of different spectral components of the pulse travelling at slightly different group velocities (GVD) [2].

2.2.1 Chromatic Dispersion

Chromatic dispersion that arises along the optical fibre is considered a non-desired effect because it limits the bandwidth and the bit-rate, beyond the propagation range. It also takes to a higher ISI. All these effects occur linearly, in the case of an SMF. CD is caused by different wavelengths travelling at different speeds through the fibre, even within the same mode [41]. This dispersion type, also known by intra-modal, is responsible for the broadening and phase shifting in the optical fibres and depends on the laser's spectral linewidth of the pulse [42]. Figure 2.18 allows a visual understanding of the CD phenomenon, where it is possible to observe the broadened pulse after cross the fibre.

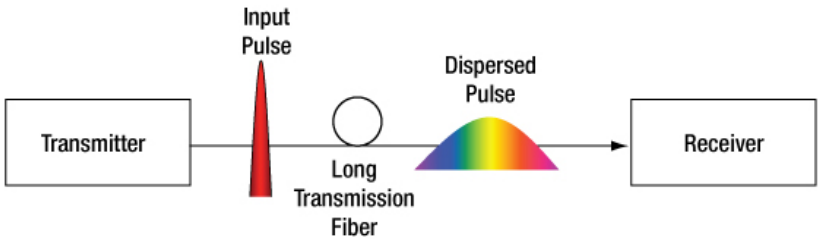

Figure 2.18: Illustration of the chromatic dispersion occurrence. [43]

Every laser oscillates within a range of wavelengths. In turn, the propagation medium, i.e. the optical fibre (fused silica), presents a refractive index varying with the signal wavelength travelling through it [41]. The higher is the signal wavelength, the lower is the refraction suffered by that signal, so longer wavelengths travel faster. Since a pulse of light from the laser usually contains several wavelengths, they tend to get spread out in time after travelling some distance across the fibre. In result, the received pulse is wider than the transmitted one, or more precisely, is a superposition of the variously delayed pulses at the different wavelengths [41].

The equation 2.15, taken from [34], is a Taylor series which affords an analytical representation for the CD phenomenon occurring at the fibre: different frequency components of an optical pulse travelling at different velocities, hence leading to the spreading of the pulse.

$$\beta(\omega) = n(\omega)\frac{\omega}{c} = \beta_0 + \beta_1\Delta\omega + \frac{1}{2}\beta_2\Delta\omega^2 + \frac{1}{6}\beta_3\Delta\omega^3 + ..., \tag{2.15}$$

$$with \quad \beta_m = \left.\frac{d^m\beta}{d\omega^m}\right|_{\omega=\omega_0}, \tag{2.16}$$

where $\beta(\omega)$ corresponds to the expansion of the mode propagation constant (also called "wave number"), ω is the angular optical carrier, and $n(\omega)$ represents the frequency-dependent refractive index of the fibre. The phase constant β_0 is inversely related with the phase velocity of the optical carrier, whose expression is $v_p = \frac{\omega_0}{\beta_0} = \frac{c}{n(\omega_0)}$. β_1 is the inverse of the group velocity that is given by $v_g = \frac{1}{\beta_1} = \left(\frac{d\beta}{d\omega}\Big|_{\omega=\omega_0} \right)^{-1}$, with β of the guided mode. The terms equal and greater than β_2 are the ones responsible for the dispersion. β_2 corresponds to the derivative of the group velocity with respect to frequency, the so-called GVD (*group velocity dispersion*). Finally, β_3 is the second order GVD and contributes to the calculations of the dispersion slope $\frac{dD}{d\lambda}$, which is an essential factor for high-speed DWDM transmission [34].

CD results of the group velocity dependence upon the frequency, applicable only to single mode waveguides. Hereupon, the CD factor of an SMF is closely related to the GVD β_2, presented in equation 2.17.

$$D = -\frac{2\pi c}{\lambda^2}\beta_2, \tag{2.17}$$

where λ is the operating wavelength. The typical values of D are in the range 15-18 $ps/nm/km$ near 1550 nm, which is the wavelength region of most interest since is where the fibre loss is minimum [2], according to what was said in chapter 1. For a typical CD factor of 17 $ps/nm/km$, β_2 is approximately -21.6 ps^2/km @ 1550 nm. This exemplary case regards a fibre exhibiting anomalous dispersion because the value of β_2 is negative. The fibre exhibits normal dispersion for $\beta_2 > 0$ or anomalous dispersion for $\beta_2 < 0$ [34].

A pulse having the spectral width of $\Delta\omega$ is broadened by $\Delta T = \beta_2 L \Delta\omega$ [34], which takes to the equation 2.18, a very common analytical way to take into account the CD.

$$\Delta t_{chr} = L \cdot D \cdot \Delta\lambda_0 = \frac{1}{\sqrt{2}\pi f_{max}}, \tag{2.18}$$

where Δt_{chr} represents the RMS pulse width at the fibre output, L the fibre length, D the dispersion parameter (whose units are $ps/nm/km$), $\Delta\lambda_0$ is spectral width, and f_{max} the maximum modulation frequency, which multiplying by L gives the signal bandwidth. Hence, the CD effect can be described as a delay of an impulse relatively to consecutive one. In physical terms, the central wavelength, λ_0, is displaced by 1 nm, after 1 km fibre propagated.

The CD is generated both from the material dispersion and waveguide dispersion. Material dispersion happens due to colours go through different speeds because the fibre refractive index varies with the wavelength. It is related to the frequency dependence of the refractive index and leads to the pulse broadening, which is typically < 0.1 ns/km, and can be reduced further by controlling the spectral width of the laser. Material dispersion sets the ultimate

limit on the bit-rate and the transmission distance. On the other hand, waveguide dispersion depends on fibre parameters such as the core radius and the index difference, Δ [2]. This one arises from the distribution of light between core and cladding [34]. The equation 2.20 refers the chromatic dispersion, which results of summing the equations 2.19.

$$D_m = -\frac{\lambda_0}{c}\frac{d^2 n_1}{d\lambda_0^2}, \qquad D_w = -\frac{n_1 \Delta}{c\lambda_0}\nu\frac{d^2(b\nu)}{d\nu^2}, \tag{2.19}$$

$$D = -\frac{\lambda_0}{c}\frac{d^2 n_1}{d\lambda_0^2} - \frac{n_1 \Delta}{c\lambda_0}\nu\frac{d^2(b\nu)}{d\nu^2}, \tag{2.20}$$

where D_m is the material dispersion, λ_0 is the central wavelength, c is the light velocity, n_1 is the refractive index of the fibre core, D_w is the waveguide dispersion, Δ is the index difference given by $\frac{n_1 - n_2}{n_1}$ (n_2 - index of the fibre cladding), ν is the normalized frequency given by $\frac{2\pi a}{\lambda_0}\sqrt{n_1^2 - n_2^2}$ (a - fibre ray), and finally D is the total/chromatic dispersion.

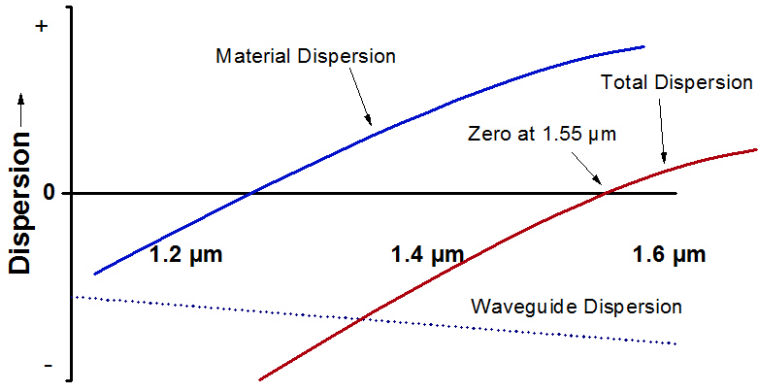

Figure 2.19: Chromatic dispersion @ 1.55 μm zero dispersion-shifted fibre. [43]

Another parameter to govern CD effects is the dispersion length L_D that corresponds to the distance after which a pulse has broadened by one bit interval. The inequation 2.21 presents the fibre length dependence upon the inverse of the squared baud-rate, B^2, upon the inverse of the squared λ_0, and upon the inverse of the absolute value of CD factor, $|D|$.

$$L \leq \frac{c}{2B^2\lambda_0^2|D|} \quad \Rightarrow \quad L_D = \frac{c}{2B^2\lambda_0^2|D|} \tag{2.21}$$

The dispersion length decreases with the bit-rate, as it is possible to conclude observing table 2.7, which regards the QPSK modulation format where the baud-rate is half of the bit-rate.

B	L_D
10 Gb/s	146.8 km
20 Gb/s	36.8 km
40 Gb/s	9.2 km

Table 2.7: Dispersion variation with bit-rate @ 1550 nm.

These lengths are much smaller than the lengths limited by ASE (*amplified spontaneous emission*) noise accumulation. For that reason, CD becomes one of the most crucial constraints for the modern high-capacity and ultra long-haul transmission optical systems.

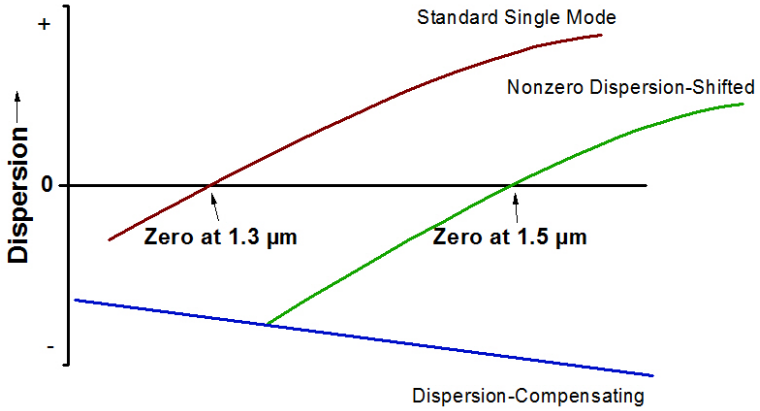

Figure 2.20: Chromatic dispersion in several fibre types. [43]

The chromatic dispersion effect, or simply GVD effect, can be mitigated in different ways such as inline compensation, following each span of the optical link by a DCF or at the receiver, digitally equalizing the accumulated dispersion of the whole optical link.

2.2.2 Amplified Spontaneous Emission

The noise is also a noteworthy constraint of a signal transmission. In optical channels, the noise is introduced by the optical amplifiers existent throughout the link. Those optical amplifiers are typically EDFAs, with gains in the region of 1550-1565 nm (C-band). As any other amplifier, EDFA adds noise and this particular case is originated from the excited Erbium ions, the so-called ASE (*amplified spontaneous emission*) [23]. The expression 2.22 is an analytical representation of that noise into an optical link and is directly associated to the figure 2.21.

$$N_o = N_A \left(e^{\alpha L_A} - 1\right) h\nu n_{sp}, \tag{2.22}$$

$$N = 2 \times N_o B, \tag{2.23}$$

where N_o is the noise spectral density per SOP, N_A is the number of amplifiers, α is the fibre loss coefficient ($0.2\ dB/km$), L_A is the distance among amplifiers, h is the Planck constant ($6.626070040\,(81) \times 10^{-34} J \cdot s$), ν is the signal frequency, and n_{sp} is the spontaneous emission factor. Hereupon, the expression 2.22 refers to a chain of N_A amplifiers periodically spaced by the fibre spans of length L_A which yields a gain of $e^{\alpha L_A}$ like is shown in figure 2.21. The expression 2.23 regards the noise power density, N, which is doubled due to the noise be double-sided white noise.

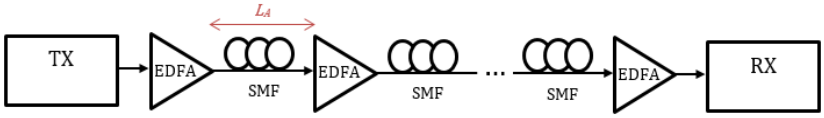

Figure 2.21: Outline of an optical communication system whose optical link consists of N_A EDFAs plus fibre spans.

The AWGN (*additive white Gaussian noise*) channel, provided by MATLAB®, is a good approximation of the optical link, if the optical power launched into each span is low. Otherwise, the channel would become nonlinear and AWGN would no longer fit as a good approximation [23]. The AWGN adds white Gaussian noise to the signal with a specified SNR, which corresponds to the *signal-to-noise ratio* per sample. The SNR is the ratio between the average signal power and average noise power and it is given in dB. As the input signal coming from the transmitter is complex, it is added complex noise, considering the signal power which is previously measured.

$$SNR = E_b/N_o + 10\log_{10}(k) - 10\log_{10}(T_{symb}/T_{samp}), \tag{2.24}$$

where E_b/N_o is the ratio of bit energy to noise spectral density, $10\log_{10}(k)$ regards the E_s/N_o which is the ratio of symbol energy to noise spectral density, whose $k = \log_2 M$[3]. Finally, the term $10\log_{10}(T_{symb}/T_{samp})$ is subtracted because the AWGN's input signal is complex, and T_{symb}/T_{samp} represents the number of samples per symbol. The figure 2.22 shows the complex low-pass equivalent of the noise PSD (*power spectral density*), $S_n(f)$, of a band-pass white noise process. In the graph, B is the noise bandwidth and N_o is the white noise power.

[3]M values 4 in the case of QPSK modulation format.

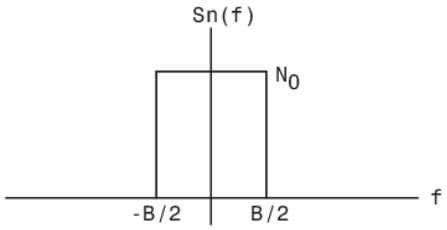

Figure 2.22: Complex low-pass noise PSD.

2.3 Receiver

The recent researching in optical communications uses optical receivers suitable to process signals modulated with complex formats and, of course, performing coherent detection. In order to approximately represent such optical circuits, it is shown in figure 1.4 a block diagram of a basic optical coherent receiver. The represented receiver circuit is once more associated to single polarization.

First of all, the receiver front-end regards the coherent detection and it is constituted by the first block, the 90° optical hybrid, plus photodetectors. The 90° optical hybrid demodulates both the received optical signal and an LO signal. Since the received signal is modulated by the modulation format QPSK, there are two components, the in-phase and quadrature, reason why the block diagram presents two branches. Photodetectors convert the two components from optical band to baseband. Then those electrical signals go through an LPF, the optical filter, and soon after through an ADC (*analog-to-digital converter*) to be oversampled, in order to become suitable for digital processing. The last three blocks (clock recovery, carrier recovery and symbol decoding) regard the digital processing which makes a complementary work of the coherent detection, compensating the impairments and, consequently, increasing the OSNR of the whole optical communication system.

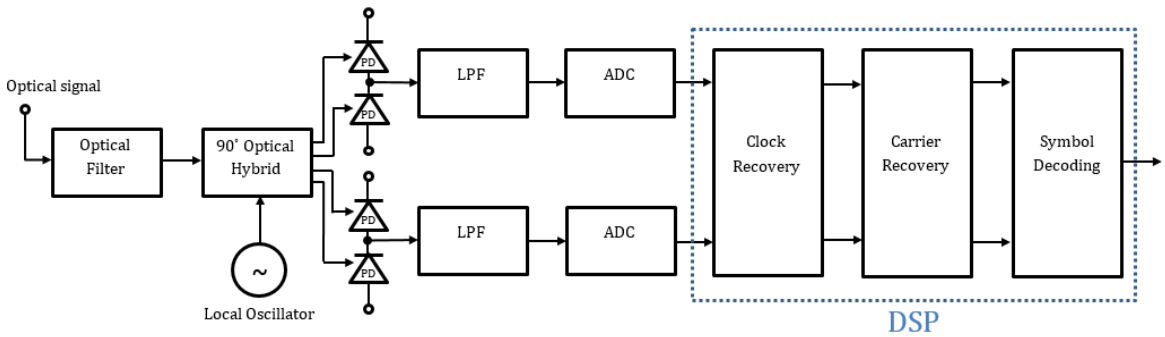

Figure 2.23: Block diagram of an overall QPSK receiver.

2.3.1 90° Optical Hybrid

In this theoretical approach of the optical receptor, it was considered a single polarization 90° optical hybrid, which is the simplest case. This device enables to extract phase and amplitude from a single polarization signal by performing four 90° phase stepped interferences between the received optical signal and an LO. It also features a phase tunability option, i.e., the 90° phase shift of the hybrid depends slightly on the wavelength being used. A 90° optical hybrid is traditionally constructed using two 50/50 beam splitters and two beam combiners, plus one 90° phase shifter. Should be noted that this component is suitable for either heterodyne and homodyne detection [44].

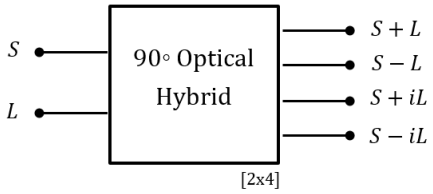

Figure 2.24: Input-output schematic of a 90° optical hybrid. [44]

As it is possible to observe in figure 2.24, a 90° optical hybrid has two inputs: one is the optical received signal (S); the other one is a local oscillator (L), used to beat or mix with the incoming signal S on the photodetector. The four outputs result of mixing the signals S and L.

2.3.2 Photodetectors

The photodetectors, or photodiodes, belong to the coherent optical receiver front-end, as well as the 90° optical hybrid. Their function is to detect the received optical signal. This stage of the reception system is responsible for turning the optical signal into an electrical one, oppositely to the IQ-modulator at the transmission side.

As figure 2.23 shows, there are considered two optical beams mixing on a photodiode (square-law detector). The used photodetectors in a receiver system can be balanced PIN photodiodes. In a PIN, it is added an intrinsic region between p and n. The intrinsic region presents a high resistivity that leads to low inverse polarizations needed for extending the depletion zone, which in turn also leads to a larger bandwidth, comparing with the simple p-n junction.

The following equations represent each photodetector output signal:

$$PD_1 = \frac{1}{4}|S|^2 + \frac{1}{8}|L|^2 + \frac{1}{2\sqrt{(2)}}SL\cos\left[(\omega_S - \omega_L)\,t + \phi(t) - \frac{\pi}{2}\right], \tag{2.25}$$

$$PD_2 = \frac{1}{4}|S|^2 + \frac{1}{8}|L|^2 - \frac{1}{2\sqrt{(2)}}SL\cos\left[(\omega_S - \omega_L)\,t + \phi(t) - \frac{\pi}{2}\right], \tag{2.26}$$

$$PD_3 = \frac{1}{4}|S|^2 + \frac{1}{8}|L|^2 + \frac{1}{2\sqrt{(2)}}SL\cos\left[(\omega_S - \omega_L)\,t + \phi(t)\right], \tag{2.27}$$

$$PD_4 = \frac{1}{4}|S|^2 + \frac{1}{8}|L|^2 - \frac{1}{2\sqrt{(2)}}SL\cos\left[(\omega_S - \omega_L)\,t + \phi(t)\right], \tag{2.28}$$

where S and ω_S are the optical received signal and respective angular frequency, L and ω_L are the local oscillator signal and respective angular frequency, and finally $\phi(t)$ is phase added upon the time.

2.3.3 Low-Pass Filter

The low-pass filter placed after the balanced photodiodes, according to the proposed reception system in [45], exists to reduce the signal bandwidth in the receiver and may have a cutoff frequency ($f_{c_{Bessel}}$) much higher than the baud-rate and much lower than the simulation bandwidth. The relation is given by 2.29 and figure 2.25 represents graphically both bandwidths. In the next Chapters' simulations, the chosen filter for this purpose was a Bessel filter, which has the particularity of having a maximally flat phase delay.

$$\frac{B_{signal}}{2} << f_{c_{Bessel}} << \frac{B_{simulation}}{2} \tag{2.29}$$

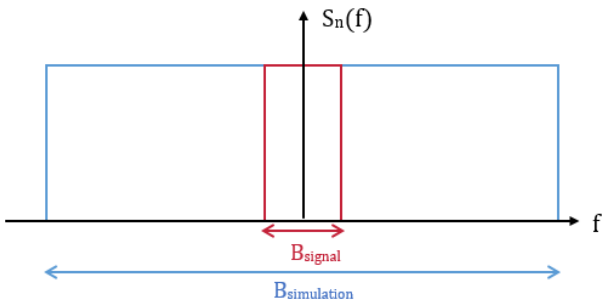

Figure 2.25: Spectrum of the signal bandwidth overlaped with the simulation bandwidth.

2.3.4 Analog-to-Digital Converter

ADC block regards the conversion of the signal from the analog domain to the digital domain, i.e. the very known sampling operation. As it was mentioned in DAC's description within the QPSK transmitter structure (Section 2.1), in computational terms, there is no continuous signal to convert, once it is not possible to digitally process continuous data. What actually happens is a signal downsampling.

2.3.5 Clock Recovery

This block is digital, i.e. belongs to the DSP part. Its goal is to synchronize the transmitter clock and receiver clock, compensating the phase and frequency shifts between them. Clock recovery block proceeds to frequency error estimation, where the error between clocks' frequency is compensated, and then proceeds also to phase adjustment, where the sampling instant of the received signal is adjusted to the ideal instant.

The clock recovery algorithm involves firstly sending the received signal into an interpolator block to smooth it, in order to facilitate the adjustment for the ideal sampling instant. After interpolation, the signal is sent to a timing estimator which, through the Gardner algorithm, yields a timing error due to its carrier independence, simple implementation and the modest oversampling requirements of two samples per symbol. The obtained error signal is then sent to a proportional integrator filter, whose proportional gain and integrator gain accommodate variations in clock phase and clock frequency, respectively. Then, an NCO (*numerically controlled oscillator*) block integrates the loop filter output in order to feedback the interpolator, returning the estimated time delay [46].

2.3.6 Carrier Recovery

Since in coherent receivers there is no phase or frequency lock in the optical domain, the transmitter and receiver lasers do not present exactly the same phase nor the same frequency. This fact yields a complex rotation of the received samples, which must be resolved through a carrier recovery block. This second block of DSP aims to compensate for the frequency shift and the phase noise between the transmitter and receiver lasers. There are various synchronization algorithms for carrier recovery, which must ensure that the complex demodulator is perfectly synchronized with the modulator. The implemented algorithms for carrier phase recovery are founded on estimator and detectors derived from maximum likelihood approach [46]. In the case of feedback structure, a temporal error provides error information of the parameter to estimate and correct it using a feedback system. On the other hand, for feedforward structure, the parameters to be corrected are estimated using a block

of observed samples and the correction is carried out on the delayed signal [47]. According to the process followed to find the algorithms, we can divide them in *Non-Data-Aided* ones and *Decision Directed* ones. In both cases, only the type of modulation must be known by the receiver. While the *Non-Data-Aided* algorithms are obtained simply by the maximization of the marginal likelihood function, the *Decision Directed* algorithms consist of estimation of the symbols by hard decisions on the received signal, then introducing them into the likelihood function beyond its maximization [46]. The maximization of the likelihood function means to get the estimator and detector expressions.

2.3.7 Symbol Decoding

The last DSP block regards the recovery of transmitted symbols from the received symbols by the application of various algorithms such as *Gardner*, *Early-Late Gate*, and *Muller & Muller* [48][49]. All these algorithms aim for estimating the optimal sampling instants. Similarly to carrier recovery stage, symbol timing recovery is based on maximum likelihood estimation, the only difference between the considered algorithms is the way they deal with TED, to approximate the adapted filter derivative [46].

Chapter 3

Chromatic Dispersion and Noise

This Chapter aims to demonstrate the impact of group velocity dispersion on a transmitted signal as well as the noise generated by the optical amplifiers. The Section 3.1 presents end-to-end simulation results of a system with CD and without noise, whereas the Section 3.2 presents simulation results for the opposite case, i.e. with noise and without CD. Then, Section 3.3 joins both channel constraints (CD and noise) in the simulations and presents their results too. All the simulations were performed in MATLAB® and the respective pseudocode excerpts lie among the graphical results. The Chapter ends in Section 3.4 with the conclusions about the results obtained, specially in a probabilistic perspective of the symbols distribution for each effect.

3.1 Propagation with CD and without Noise

This Section is exclusively dedicated to the chromatic dispersion effect over the transmitted signal. Therefore, there was considered the analytical representation of such phenomenon. The GVD of an optical fibre results of a parabolic phase profile on its frequency response.

$$H_c(\omega) = e^{-\frac{i\omega^2\beta_2 L}{2}}, \tag{3.1}$$

where β_2 is the GVD and L is the fibre length.

In spite of being an optical system, the signal never gets to be processed at an optical-band because it is intended to have an ideal system. So the transmitter does not simulate the modulation of an optical carrier and that means the signal remains at baseband, i.e. radio-frequency. Without IQ-modulation, it is possible to have an ideal signal once it does not suffer attenuation from the modulator. Consequently, at the receiver side, the optical front-end is not simulated too, because the received signal is already at baseband. The signal

that goes into the optical fibre is complex, whose conversion is made soon by the mapper block. The optical channel is simulated through the linear response, represented by equation 3.1, which is based on [2].

Below, it is presented the result of an exemplifying simulation of a propagation affected by CD, considering $D = 17\ ps/nm/km$, the value of the dispersion parameter at 1550 nm in a standard SMF. The figure 3.1 allows visualizing the CD effect in the constellation of the received signal for different fibre lengths against the original constellation. Right after, it is the pseudocode that produced that set of figures.

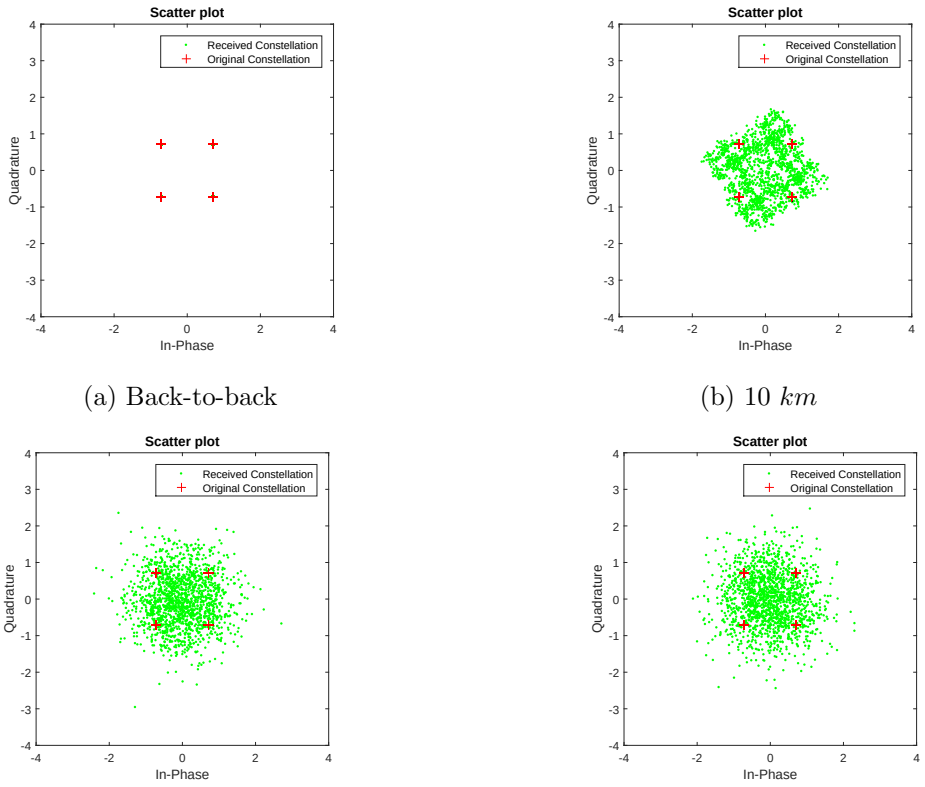

(a) Back-to-back

(b) 10 km

(c) 100 km

(d) 1000 km

Figure 3.1: Constellations resulting of different optical fibre lengths.

```
D = 17*1e-6;
L = [0  10*1e+3  100*1e+3  1000*1e+3];
lambda = 1550*1e-9;
c = 299792458;
Hc = exp((1i*2*pi*D*L*lambda^2*f.^2)/c);
rxSignal = Hc.*txSignal;
```

First of all, it is important to make a brief description of the general simulation, which is used in this and also in the next Sections, in order to state the simulation input values.

The PM-QPSK transmission system is simulated considering a bit-rate of 100 Gb/s, then 50 Gb/s per SOP. As QPSK modulation format is applied, the symbol-rate per SOP is 25 $Gsymb/s$, to which one is added 3 $Gsymb/s$ exclusively for FEC, resulting of 28 $Gsymb/s$. In every simulation it is considered only one polarization, so the transmission system is in fact a QPSK transmission system whose signal presents a symbol-rate of 28 $Gsymb/s(1+\beta)$, where β (rolloff factor of the pulse shaper) values 0. The goal is to simplify the system as much as possible in order to focus merely on the GVD effect. The number of samples per symbols to simulate system is 32, which results of 896 GHz of simulation bandwidth - $32samp/symb \times 28Gsymb/s$. In the receiver, this fact takes to have a low-pass filter with a cutoff frequency that lies between 14 GHz and 448 GHz, and still sufficiently far from each of the two values, according to the relation in 2.29. The chosen value for the Bessel filter's cutoff frequency was then 100 GHz.

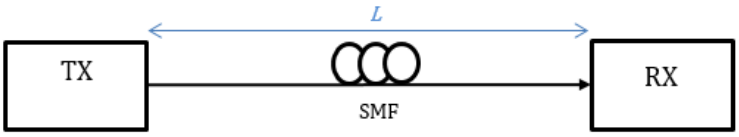

Figure 3.2: Block diagram of a transmission system whose optical channel is composed only by an L length SMF - propagation with CD and without noise.

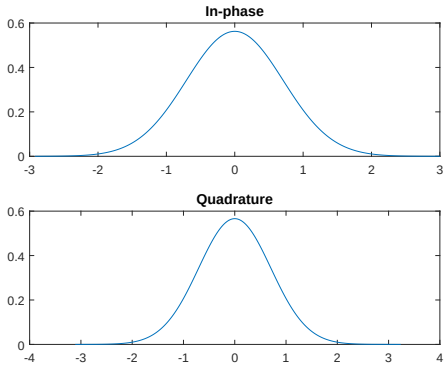

Figure 3.3: Normal PDF for in-phase and quadrature data components correspondent to the simulation of figure 3.1d (1000 km fibre).

```
Ix_received = real(rxSignal);              % In-phase symbols
Qx_received = imag(rxSignal);              % Quadrature symbols
normIx = normpdf(sort(Ix_received),0,std(Ix_received));
normQx = normpdf(sort(Qx_received),0,std(Qx_received));
```

By the figure 3.3 it is possible to observe that their distribution probability for both components tend to a Bell curve, which is the shape of a Gaussian function, and analytically proved later in this Chapter. In statistics, Gaussian function corresponds to the PDF (*probability density function*) of the normal distribution and it is given by the next equation, where x is the vector of samples, σ is the standard deviation, μ is the mean, and σ^2 is the variance:

$$f_G(x) = \frac{1}{\sigma\sqrt{2\pi}} e^{-(x-\mu)^2/(2\sigma^2)}. \tag{3.2}$$

The next simulation results were yielded by a MATLAB script whose the code is in C.1 and regards a propagation set-up represented by figure 3.2, where the fibre length L takes several values: 0 km, 1 km, 10 km, 100 km, 1000 km. The constellation diagrams show how the chromatic dispersion increase, resulting of the fibre length increase, affects the symbols distribution.

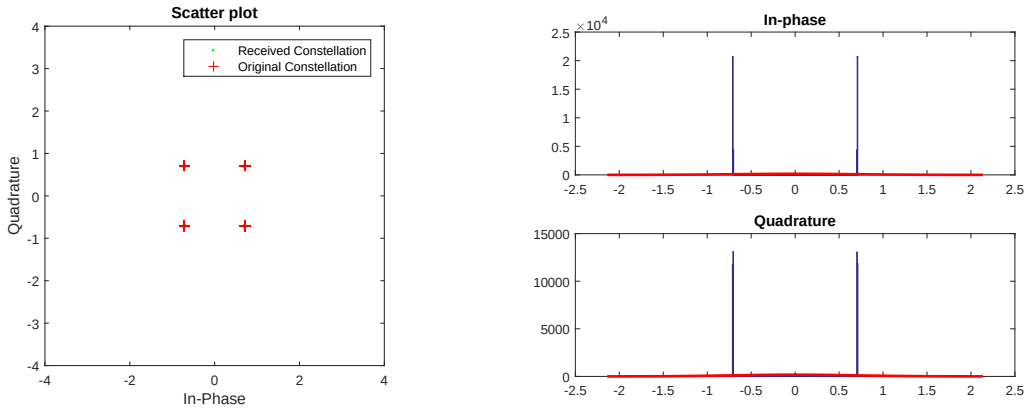

Figure 3.4: $L = 0$ km - back-to-back.

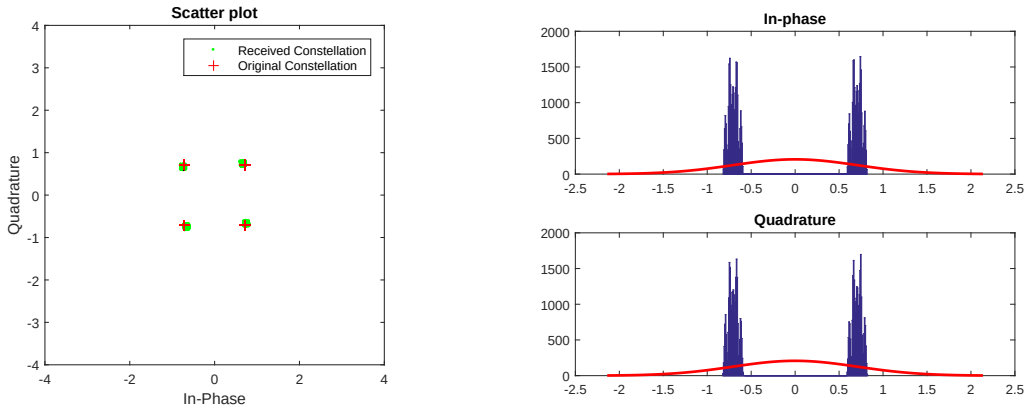

Figure 3.5: $L = 1$ km.

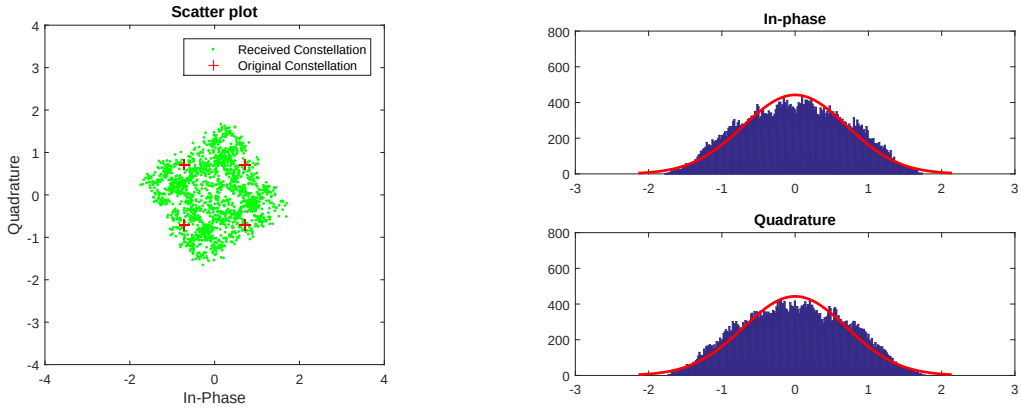

Figure 3.6: $L = 10\ km$.

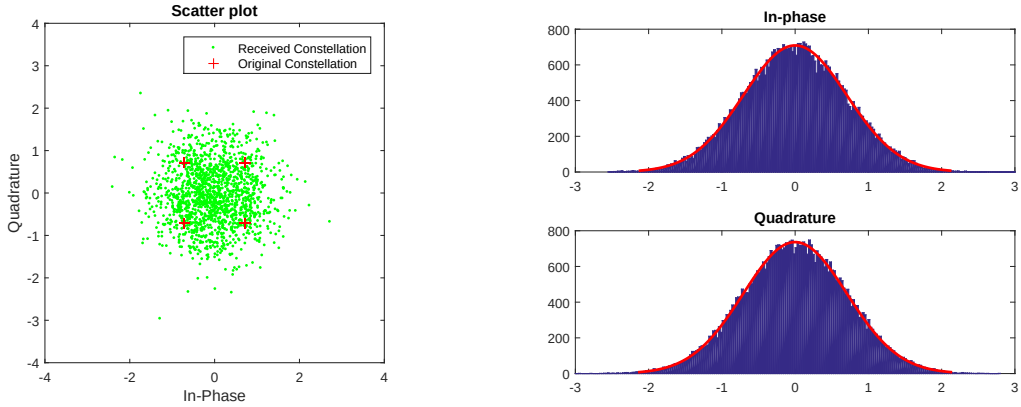

Figure 3.7: $L = 100\ km$.

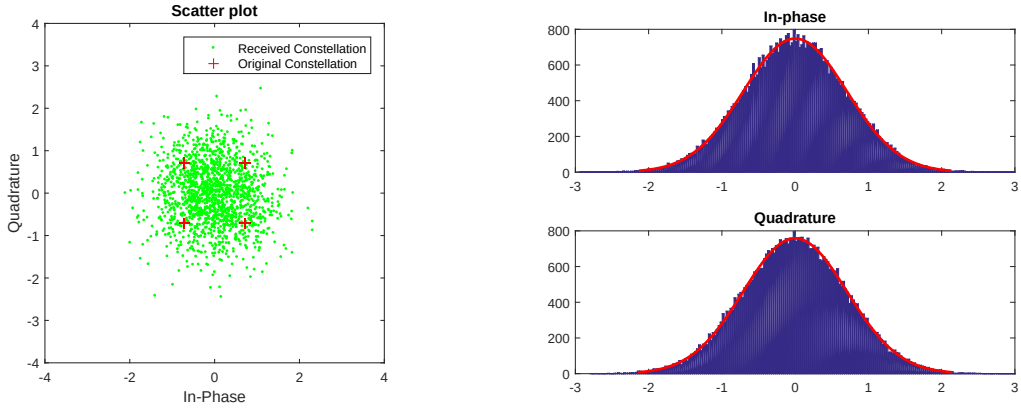

Figure 3.8: $L = 1000\ km$.

```
%%%%%%%%%%%%%%%% Scatter plot %%%%%%%%%%%%%%%%
h = scatterplot(rxSymbols,numSamplesPerSymbol,0,'g.');  % In-phase symbols
scatterplot(txSymbols,numSamplesPerSymbol,0,'r+',h);    % Quadrature symbols
```

```
%%%%%%%%% Histogram fit plot %%%%%%%%%
Ix_received = real(rxSignal);    histfit(Ix_received);    % In-phase symbols
Qx_received = imag(rxSignal);    histfit(Qx_received);    % Quadrature symbols
```

The graphs existent on the right side of each constellation are histograms fitted by a normal density function regarding the symbols distribution. If the red line curve have a bell shape, it means the symbols come from a normal distribution.

In order to evaluate the distribution probability of the symbols on the complex plan, there were taken the variance values of each component, σ_I^2 and σ_Q^2 for all the fibre lengths. The variance results of:

$$\sigma^2 = \sum_i \frac{(x_i - \overline{x})^2}{N} \quad , \tag{3.3}$$

$$where \qquad \overline{x} = \sum_i \frac{x_i}{N} \quad . \tag{3.4}$$

Thereby, both previous equations are statistical parameters. Equation 3.3 corresponds to the variance of a dataset, whereas equation 3.4 corresponds to its mean value.

L	σ_I^2	σ_Q^2
0 km	0.5000	0.5000
1 km	0.4999	0.5001
10 km	0.5008	0.4992
100 km	0.4977	0.5022
1000 km	0.4971	0.5019

Table 3.1: Variances of I and Q components upon fibre lengths.

Posteriorly, it was proceeded to the Kolmogorov-Smirnov test, which provides the goodness of fit of a cumulative distribution regarding to a specified one. This test basically measures how much does the symbols distribution fit in a normal plot, i.e. how much do the symbols come from a normal distribution. The cumulative of a random sample of N elements is expected to be fairly close to a specified distribution function, which in this case is a Gaussian function. If it is not close enough, then the cumulative distribution of the random sample is not Gaussian. The Kolmogorov-Smirnov test bases on the maximum difference between the empirical and the hypothetical cumulative distribution [50].

The respective MATLAB function *KS-Test* returns the 'h-value' as a test decision for the null hypothesis that the data come from a standard normal distribution. Null hypothesis is a type of hypothesis used in statistics that proposes that no statistical significance exists in a set of samples. Thereby, the null hypothesis assumes that any kind of difference or significance observed in a set of data is due to chance. The conjecture works for a certain significance level that, in the case of *KS-Test* function, is set to 5% by default. The MATLAB function can return a second value, 'p-value', that is the level of marginal significance within a statistical hypothesis test, such as the Kolmogorov-Smirnov test. The 'p-value' represents the smallest level of significance at which the null hypothesis would be rejected in favour to the alternative hypothesis. The 'p-value' must be higher than 0 and lower than 1. The test returns 'h=1' for a significance level higher than 'p-value', otherwise it returns 'h=0' that means the *KS-Test* fails to reject the null hypothesis at the set significance level.

```
[h,p] = kstest(Ix_received);     % default significance level: 0.05
[h,p] = kstest(Qx_received);     % default significance level: 0.05
```

L	σ_I^2		σ_Q^2	
	h	p	h	p
0 km	1	0	1	0
1 km	1	0	1	0
10 km	1	0	1	0
100 km	1	4.45E-260	1	1.99E-263
1000 km	1	3.55E-304	1	2.11E-299

Table 3.2: Results from the *KS-Test* for the all scenarios of fibre length.

L	σ_I^2		σ_Q^2	
	h	p	h	p
0 km	1	0	1	0
1 km	1	0	1	0
10 km	1	0	1	0
100 km	1	~ 0	1	~ 0
1000 km	1	~ 0	1	~ 0

Table 3.3: Same results from table 3.2.

There is 'p=0' for the whole cases, which deprecates completely the Kolmogrov-Smirnov test for these simulation scenarios, once there is no significance level associated.

Finally, there were observed the eye diagrams of signal before and after the fibre for the last scenario, when the GVD is mostly noted.

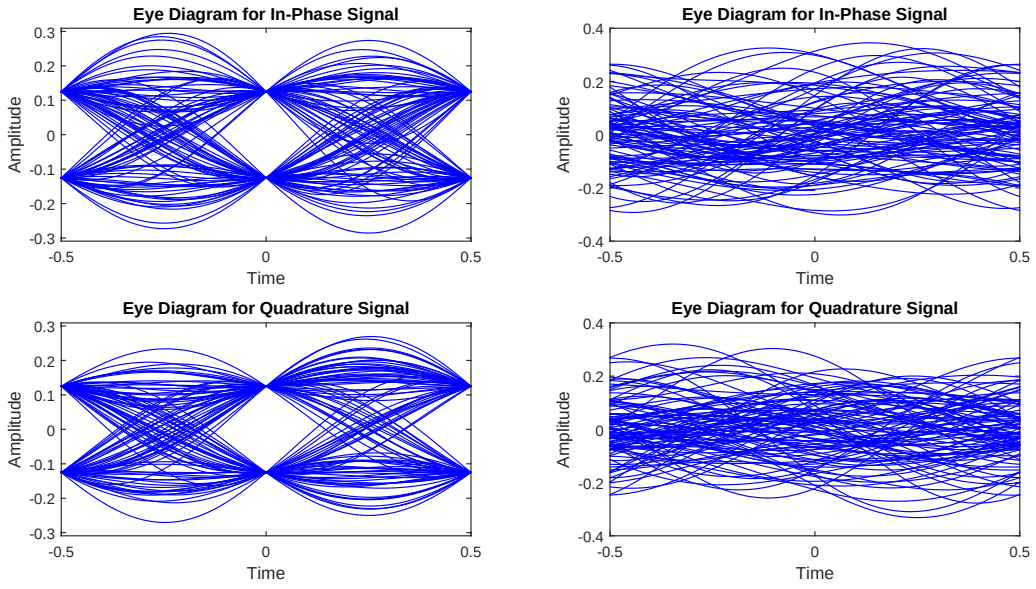

(a) Transmitted signal (b) Received signal

Figure 3.9: Eye diagrams of the transmitted signal and the received signal after cross a 1000 km fibre, with linear GVD effect.

```
initial = span/2*numSamplesPerSymbol+1;
final = initial + 200*numSamplesPerSymbol;
eyediagram(txSignal(initial:final),numSamplesPerSymbol*2);
eyediagram(rxSignal(initial:final),numSamplesPerSymbol*2);
```

3.2 Propagation with Noise and without CD

This Section treats the noise effect throughout the optical channel, without considering the GVD. Thereby, it is supposed to simulate exclusively the optical amplifiers, i.e. without the SMF spans. For than reason, and as it was mentioned in the Section 2.2.2, several EDFAs can be simulated by only one AWGN channel MATLAB function. This block allows defining the noise level through the E_b/N_o: ratio of bit energy to noise spectral density. This ratio represents a normalized SNR measure, where E_b is the energy per bit and N_o is the noise spectral density.

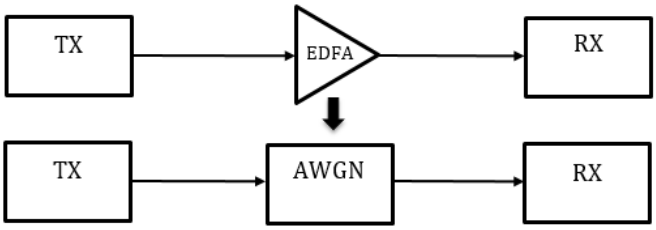

Figure 3.10: Block diagram of a transmission system whose optical channel is composed only by an AWGN channel - propagation with noise and without CD.

The next simulation results were yielded by a MATLAB script whose the code is in C.2 and regards a propagation set-up represented by figure 3.10, where the AWGN channel takes several values for E_b/N_o: 15 dB, 10 dB, 5 dB, 0 dB, -5 dB. The constellation diagrams show how the noise increase affects the symbols distribution at the receiver side.

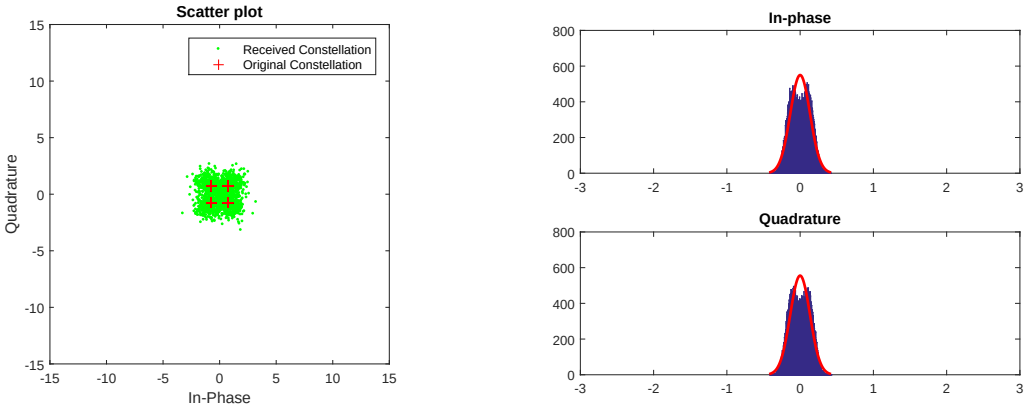

Figure 3.11: $E_b/N_o = 15\ dB$.

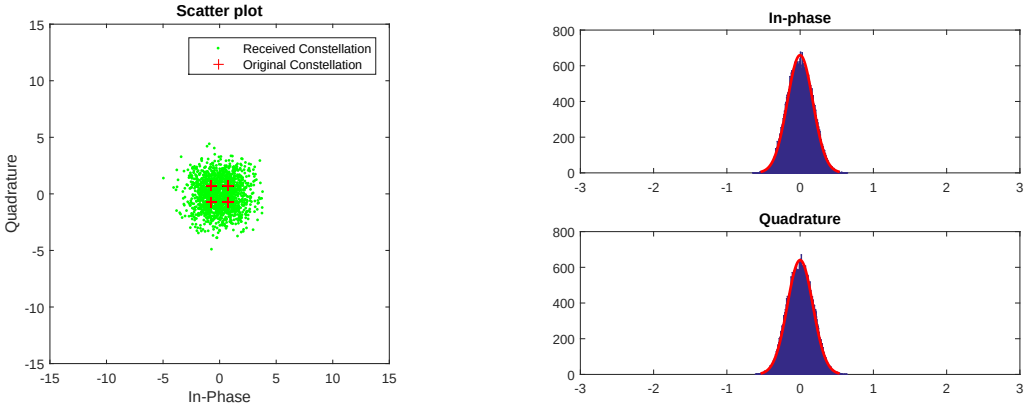

Figure 3.12: $E_b/N_o = 10\ dB$.

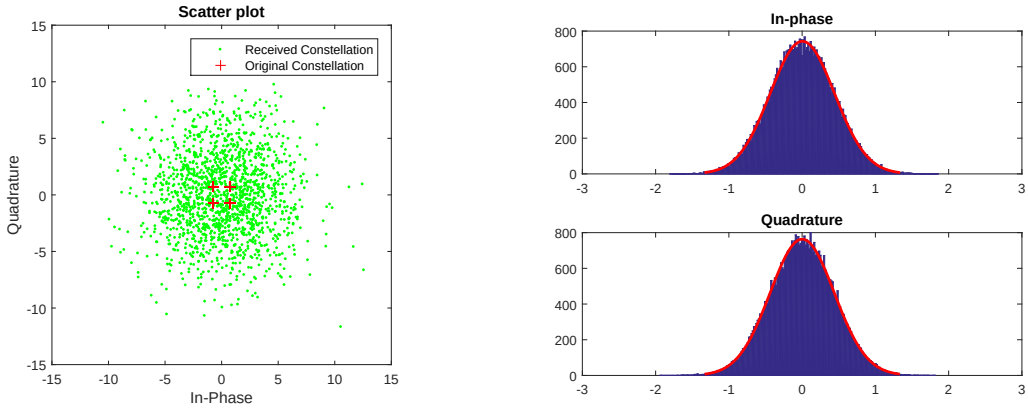

Figure 3.13: $E_b/N_o = 5\ dB$.

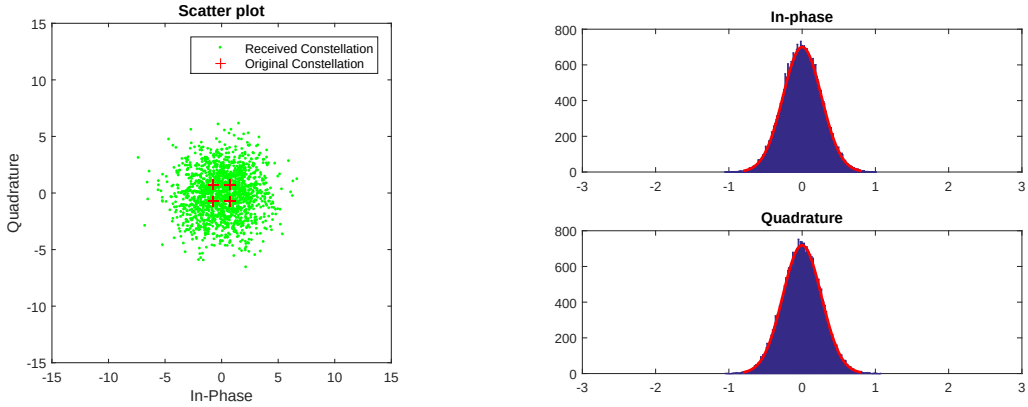

Figure 3.14: $E_b/N_o = 0\ dB$.

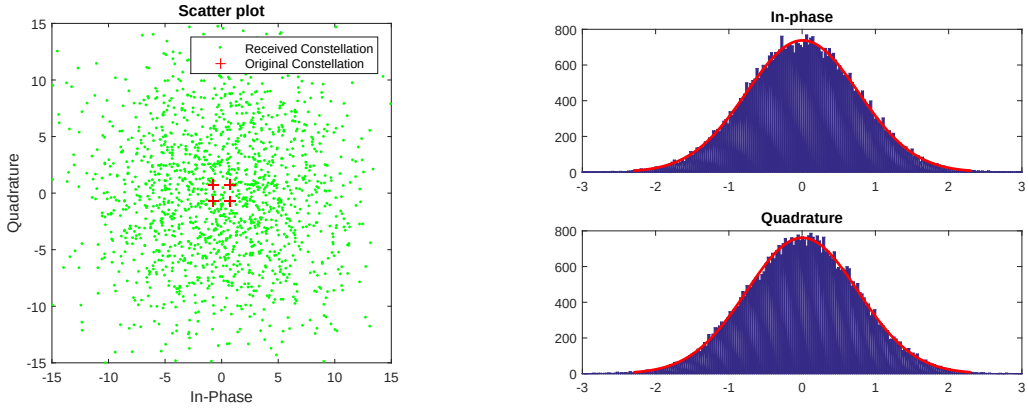

Figure 3.15: $E_b/N_o =$ -5 dB.

```
EbNo = [15 10 5 0 -5];                                    % dB
SNR = EbNo + 10*log10(k) - 10*log10(numSamplesPerSymbol);  % dB
rxSignal = awgn(txSignal, SNR, 'measured');
```

Similarly to the received symbols distribution resulting of GVD, also the noise causes a Gaussian symbols distribution as figure 3.16 shows. Right after, it is presented also the variances table 3.4 for each simulated scenario, for both in-phase and quadrature components, as well as the eye diagrams (figure 3.17).

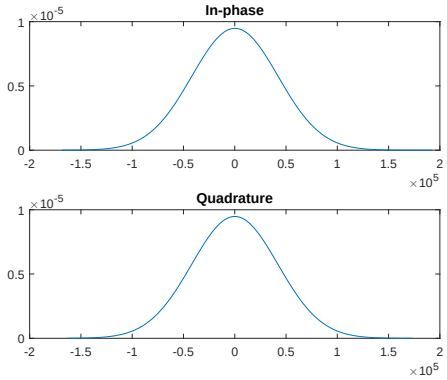

Figure 3.16: Normal PDF for in-phase and quadrature data components correspondent to the simulation of figure 3.15 (-5 dB of E_b/N_o).

E_b/N_o	σ_I^2	σ_Q^2
15 dB	0.0182	0.0180
10 dB	0.0304	0.0303
5 dB	0.0689	0.0685
0 dB	0.1905	0.1922
-5 dB	0.5820	0.5784

Table 3.4: Variances of I and Q components upon E_b/N_o values.

E_b/N_o	σ_I^2		σ_Q^2	
	h	p	h	p
15 dB	1	0	1	0
10 dB	1	0	1	0
5 dB	1	0	1	0
0 dB	1	0	1	0
-5 dB	1	0	1	0

Table 3.5: Results from the *KS-Test* for the all scenarios of E_b/N_o.

Once again, there is 'p=0' for the whole cases which means that any scenario fails the *KS-Test*.

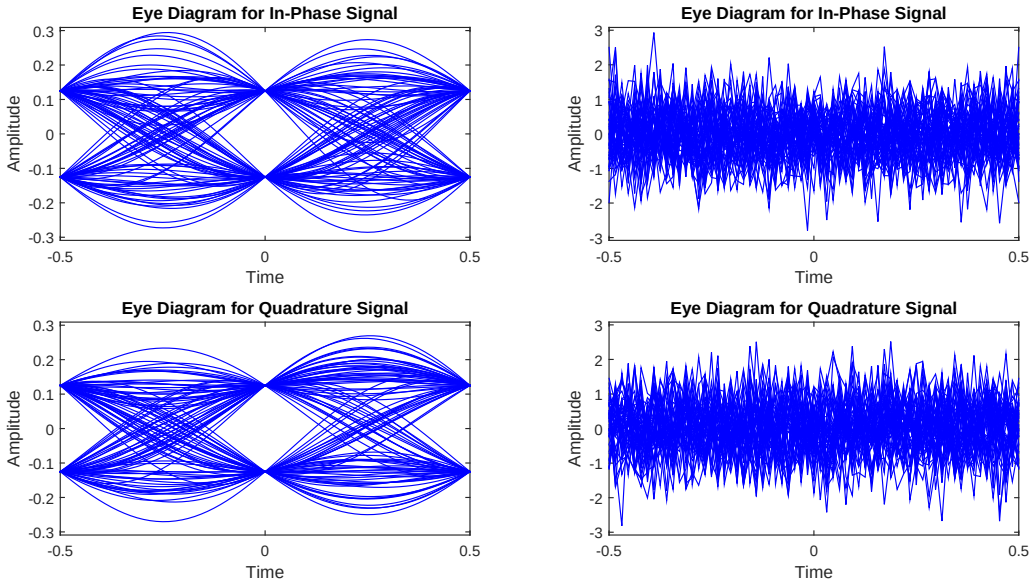

(a) Transmitted signal

(b) Received signal

Figure 3.17: Eye diagrams of the transmitted signal and the received signal after cross an AWGN channel where $E_b/N_o = -5dB$.

3.3 Propagation with CD and Noise

In this case, the goal consists of observing the GVD and the ASE simultaneously. The equation 2.22, previously mentioned in the Section 2.2.2, is the basis to the current simulation propagation, represented by figure 3.18.

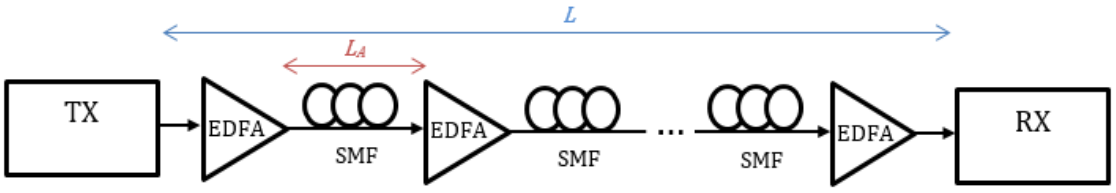

Figure 3.18: Block diagram of a transmission system whose optical channel is composed by N_A EDFAs splitting L_A length SMF spans - propagation with CD and with noise.

The next simulation results were yielded by a MATLAB script whose the code is in C.3 and regards a propagation set-up where the number of optical amplifiers, also called regenerators takes several values: 0, 1, 5, 10, 50. The regenerators split SMF spans of 100 km. The constellation diagrams show how the chromatic dispersion combined with the noise increase affects the symbols distribution.

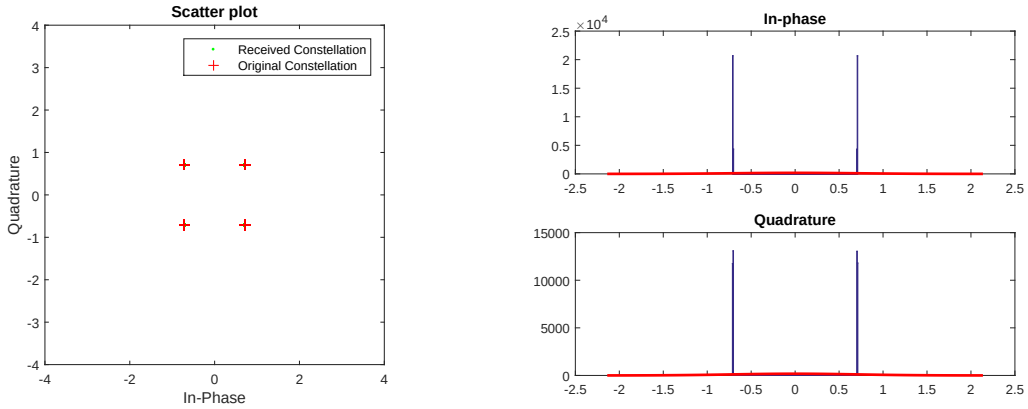

Figure 3.19: $N_A = 0$.

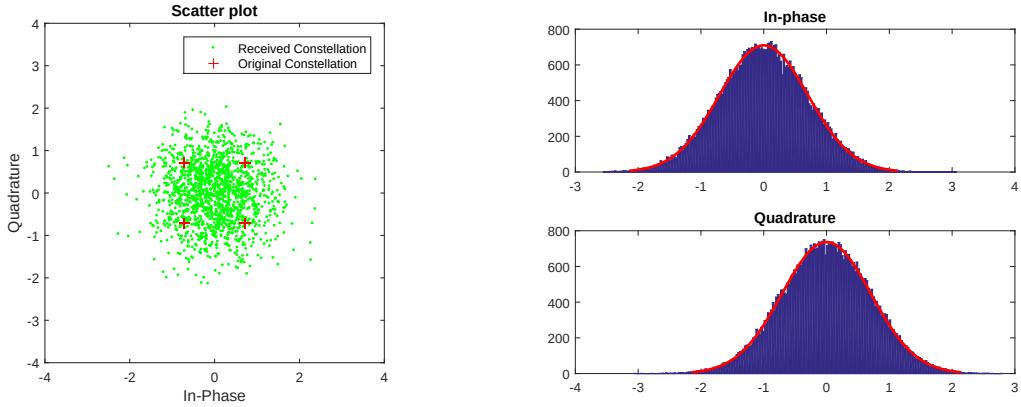

Figure 3.20: $N_A = 1$.

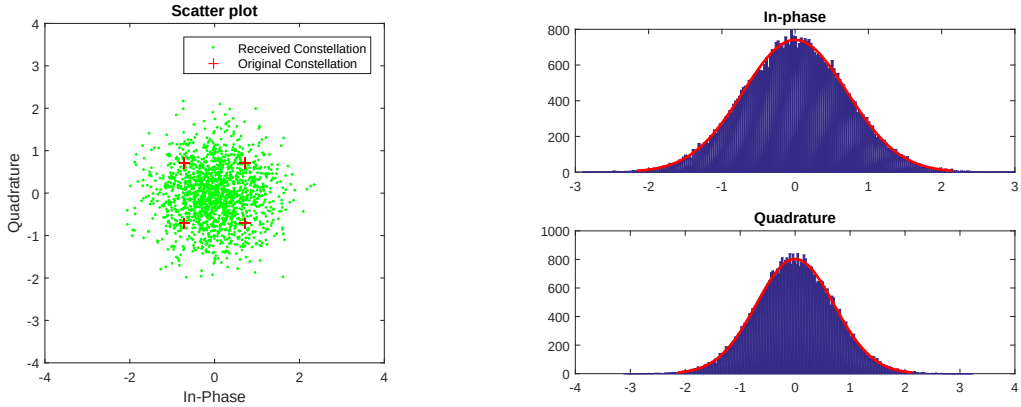

Figure 3.21: $N_A = 5$.

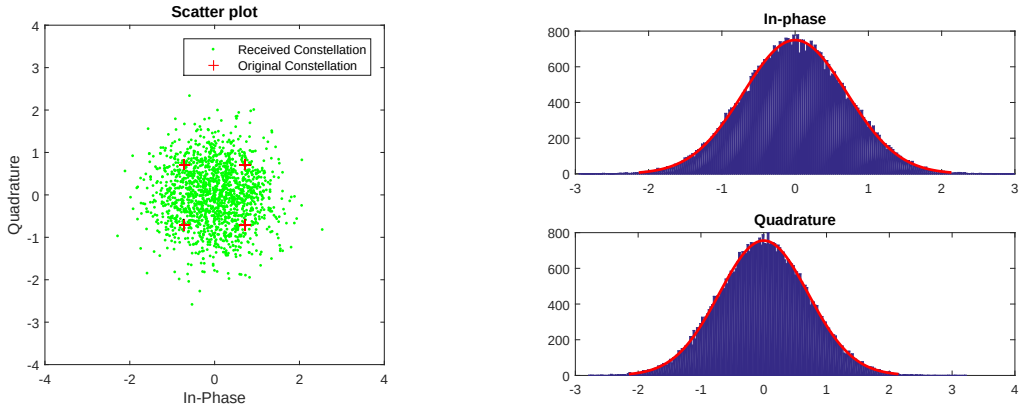

Figure 3.22: $N_A = 10$.

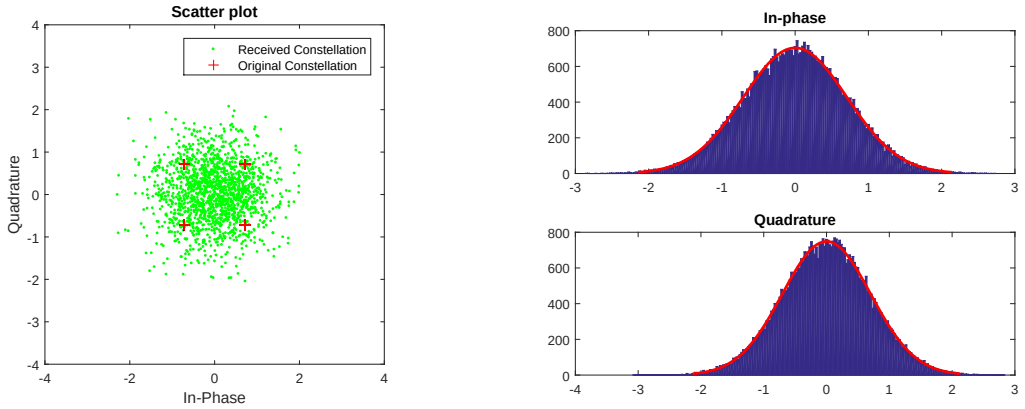

Figure 3.23: $N_A = 50$.

```
D = 17*1e-6;                          % s/nm/m
L = [0 100e3 500e3 1000e3 5000e3];    % Total length
La = 100e3;                           % Span length
Na = L/La;                            % Number of EDFAs/spans
alpha = 0.2e-3;                       % Loss coefficient
gain = 10^(alpha*La/10);              % Linear gain
hP = 6.62607004*1e-34;                % Planck constant
nsp = 1;                              % Spontaneous emission factor
lambda = 1550*1e-9;                   % m
c = 299792458;                        % m/s
v = c/lambda;                         % Hz

Hc = exp((1i*2*pi*D*L*lambda^2*f.^2)/c);
rxSignal = Hc.*txSignal;              % GVD
```

```
NSD = Na*(gain - 1)*v*hP*nsp;              % Noise spectral sensity
N_optical_power = 2*NSD * fs;              % Noise power density
noise_I = sqrt(N_optical_power/2);
noise_Q = sqrt(N_optical_power/2);

noise = noise_I + 1i * noise_Q;            % ASE
rxSignal = rxSignal + noise;
```

Once again, there are presented the PDF graphs for in-phase and quadrature components taken from the most Gaussian distribution obtained. There are also presented the variances tables whose results were taken with the purpose of evaluating the distribution evolution across the different number of fibre spans. The first one, 3.6, contains the variances results from the propagation affected by GVD and ASE separately, while the third one, 3.8, contains the variances from the same propagation affected by both effects simultaneously. The second table, 3.7, contains the sum of the variances from the table 3.6, to which it is subtracted '0.5000', represented by σ^2_{ini}. This value corresponds to the initial variance of the symbols distribution, i.e. without suffering any effect, so it has to be accounted only once. For better understanding, the standard deviation of the symbols, σ_{ini}, equals the module of their original coordinates for each component.

$$\sigma_{ini} = \frac{\sqrt{2}}{2} \quad \Longrightarrow \quad \sigma^2_{ini} = \frac{1}{2} \tag{3.5}$$

N_A	$\sigma^2_{I_{GVD}}$	$\sigma^2_{Q_{GVD}}$	$\sigma^2_{I_{ASE}}$	$\sigma^2_{Q_{ASE}}$
0	0.5000	0.5000	0.5000	0.5000
1	0.4977	0.5022	0.5000	0.5000
5	0.5029	0.4966	0.5000	0.5001
10	0.4971	0.5019	0.5002	0.5002
50	0.5002	0.4947	0.5007	0.5007

Table 3.6: Variances upon number of amplifiers for separated simulations of GVD and ASE respectively.

$\sigma^2_{I_{GVD}} + \sigma^2_{I_{ASE}} - \sigma^2_{ini}$	$\sigma^2_{Q_{GVD}} + \sigma^2_{Q_{ASE}} - \sigma^2_{ini}$
0.5000	0.5000
0.4977	0.5022
0.5029	0.4967
0.4973	0.5021
0.5009	0.4954

Table 3.7: Sum of the variances from the previous table for both components I and Q, subtracting σ^2_{ini}.

N_A	σ_I^2	σ_Q^2
0	0.5000	0.5000
1	0.4978	0.5002
5	0.5029	0.4967
10	0.4974	0.5021
50	0.5009	0.4951

Table 3.8: Variances of I and Q components upon number of amplifiers.

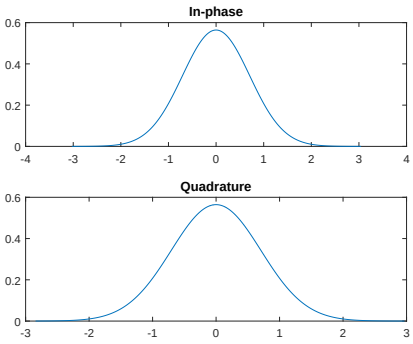

Figure 3.24: Normal PDF for in-phase and quadrature data components correspondent to the simulation of figure 3.23 (50 regenerators).

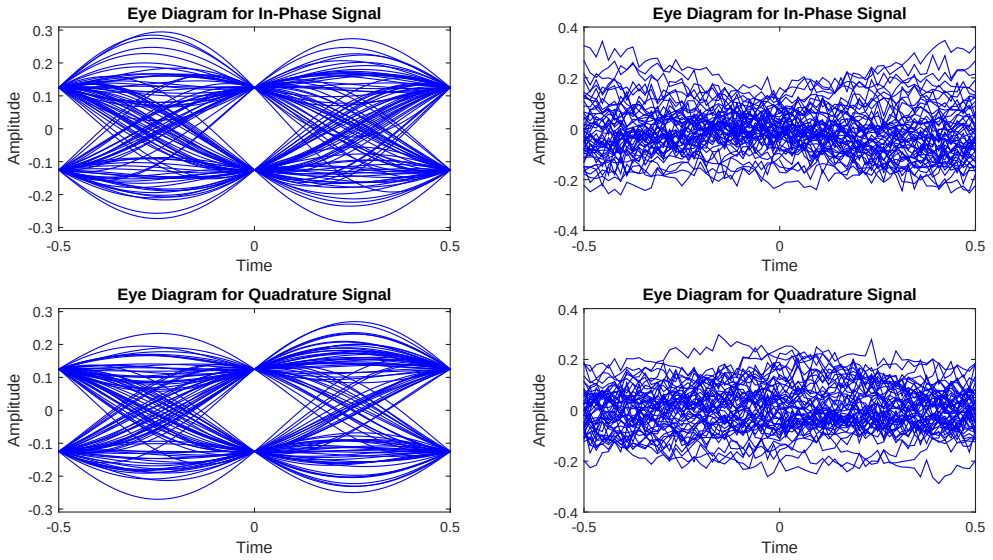

(a) Transmitted signal

(b) Received signal

Figure 3.25: Eye diagrams of the transmitted signal and the received signal after cross an optical channel with 50 EDFAs splitting 100 km fibre spans.

3.4 Conclusions

After simulating the three propagation scenarios and taking the respective evaluation graphics and values, it is possible to compare them in order to get some conclusions about the behaviour of the received signal. The GVD value increases with the fibre length, whereas the noise increases with the SNR value decrease.

As it was mentioned already throughout the Chapter, the received signal for each one of the three propagations presents a symbols distribution with Gaussian characteristics. Both the GVD and ASE yield signals whose symbols distribution tend to a Gaussian distribution. This conclusion is suitable for the case when the two phenomenons occur separately, but also when they occur simultaneously. The Gaussian distribution can be graphically proved by the constellations, histograms and normal plots. On the other hand, the Gaussian symbols distribution is mathematically complemented by the *KS-Test*, whose results are given in each propagation scenario. It is not possible in any case to achieve a measurable value for goodness of fit. That means that the yielded symbols distribution is not Gaussian enough to take into account the *goodness of fit* concept in any propagation scenario. Regarding the eye diagrams, in the case of the GVD effect it is obtained an eye digram with ISI, which can be considered one more evidence of signal distortion by chromatic dispersion. By comparison of the tables 3.8 and 3.7, it is possible to conclude that a propagation affected by GVD and ASE at the same time generates a symbols distribution with variance approximate to the sum of the variances of the symbols distributions generated by GVD and ASE affecting the propagation in a single way.

$$\sigma_I^2 \approx \sigma_{I_{GVD}}^2 + \sigma_{I_{ASE}}^2 - \sigma_{ini}^2 \tag{3.6}$$

$$\sigma_Q^2 \approx \sigma_{Q_{GVD}}^2 + \sigma_{Q_{ASE}}^2 - \sigma_{ini}^2 \tag{3.7}$$

Chapter 4

Digital Equalization and Filtering

In this Chapter, there is a simultaneous concern about the chromatic dispersion mitigation and about trying to eliminate the noise from the received signal as much as possible, so the binary signal can be received with the lowest number of errors. The structure of the current Chapter is organized into four Sections in parallel with the Sections of the Chapter 3. So Section 4.1 covers the digital CD equalization of a system that does not consider noise. In turn, Section 4.2 deals with the noise filtering of a system that does not feature CD. These performances were simulated once again with MATLAB®. The graphical results are followed by pseudocode excerpts likewise the previous Chapter. The Section 4.3 joins both digital blocks (equalization and filtering) as in Section 3.3. At last, Section 4.4 lists the conclusions taken from the simulation results obtained throughout the current Chapter.

4.1 Linear Equalization of a Propagation without Noise

In this Section, it is presented the CD equalization of the propagation treated in Section 3.1. Once the signal propagated is affected by a linear effect and its response is known, it is proposed the application, at the receiver, a filter with the inverse response of equation 3.1, which is given by:

$$H_1(\omega) = [H_c(\omega)]^{-1} = \frac{1}{e^{-\frac{i\omega^2\beta_2 L}{2}}} \quad . \tag{4.1}$$

Below, there are placed the figures 4.4 resulting from the same simulations from 3.1, but now applying the linear equalizer H_1. This linear filter is represented in figure 4.2, taking part of the DSP context in the receiver. The respective code lies in the Appendix C.4.

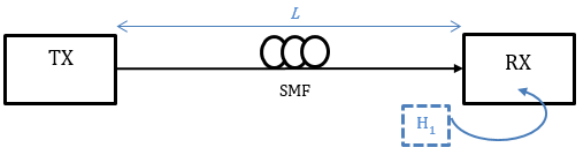

Figure 4.1: Block diagram of a transmission system whose receiver performs CD equalization.

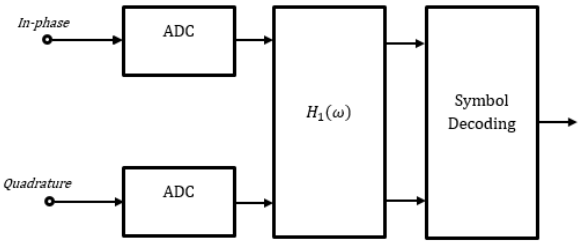

Figure 4.2: Block diagram of the receiver in detail, containing the filter $H_1(\omega)$.

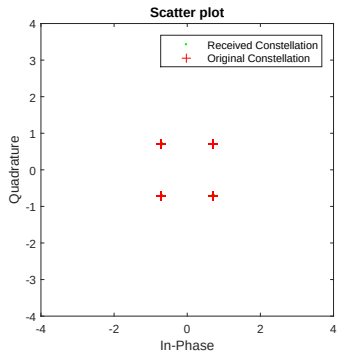

(a) Back-to-back

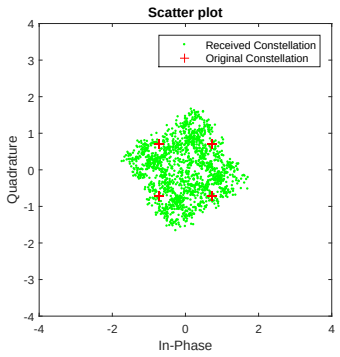

(b) 10 km

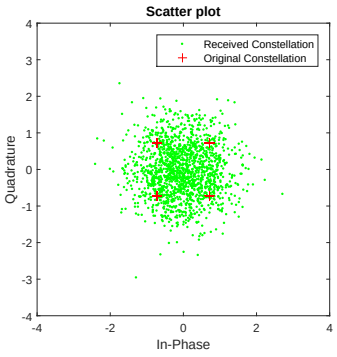

(c) 100 km

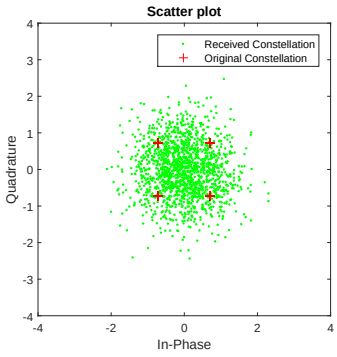

(d) 1000 km

Figure 4.3: Constellations resulting of different optical fibre lengths before linear equalization is applied.

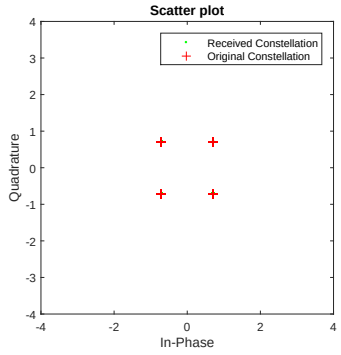

(a) Back-to-back

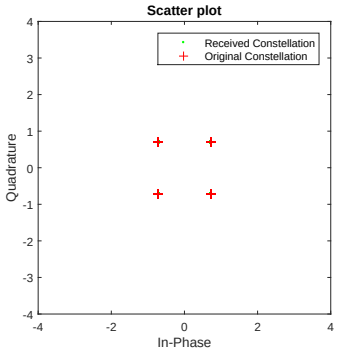

(b) 10 km

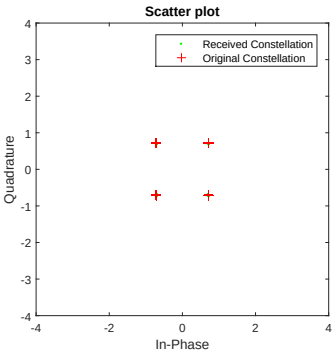

(c) 100 km

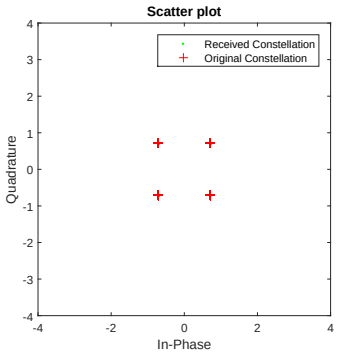

(d) 1000 km

Figure 4.4: Same constellations after linear equalization is applied.

4.2 Matched Filtering of a Propagation with Noise and without CD

Following the same line of though than the previous Section, it is proposed a linear filter to compensate the noise in the propagation studied in 3.2. The taken solution was then the *matched filter*, because it is the optimal detection scheme in the maximum-likelihood sense. This type of filter is capable of producing the maximum achievable instantaneous SNR at its output when a signal plus additive noise corresponds to the input, and the noise does not need to be Gaussian [51]. The respective code of the simulation is in Appendix C.5.

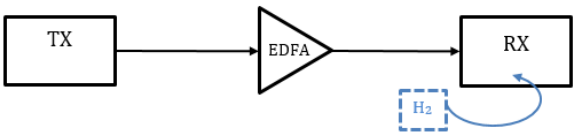

Figure 4.5: Block diagram of a transmission system whose receiver performs matching filtering, in order to eliminate part of the noise.

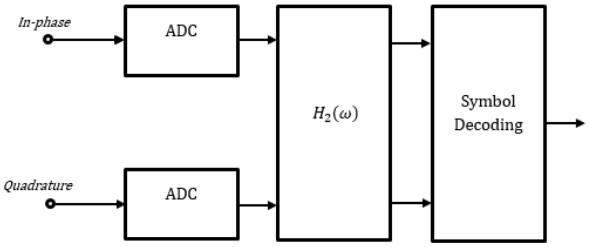

Figure 4.6: Block diagram of the receiver in detail, containing the filter $H_2(\omega)$.

The matched filtering was made using the RRC filter whose impulse response corresponds to equation 2.5, presented in the Chapter 2. Noteworthy that the rolloff factor used for these propagations was always '0' ($\beta = 0$), so the pulse shape response corresponds to the rectangular one. The following constellation diagrams show the signal enhancement with the usage of this digital processing.

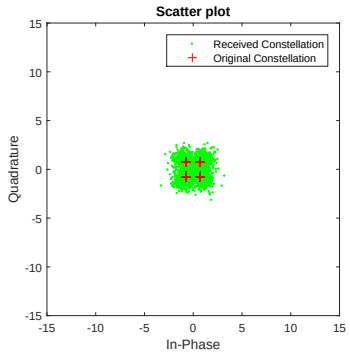

(a) 15 dB

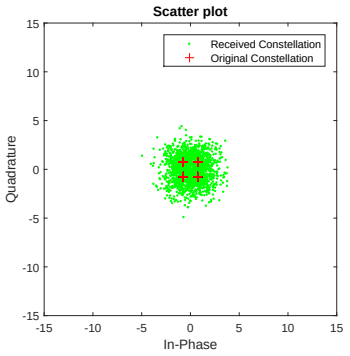

(b) 10 dB

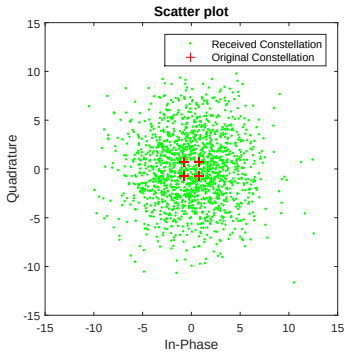

(c) 5 dB

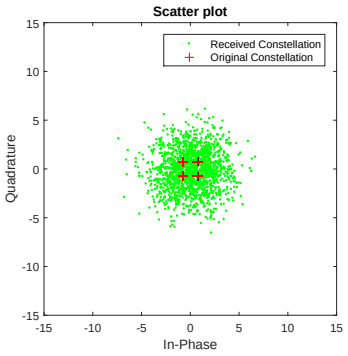

(d) -5 dB

Figure 4.7: Constellations resulting of different values of ratio of bit energy to noise spectral density before matched filtering is applied.

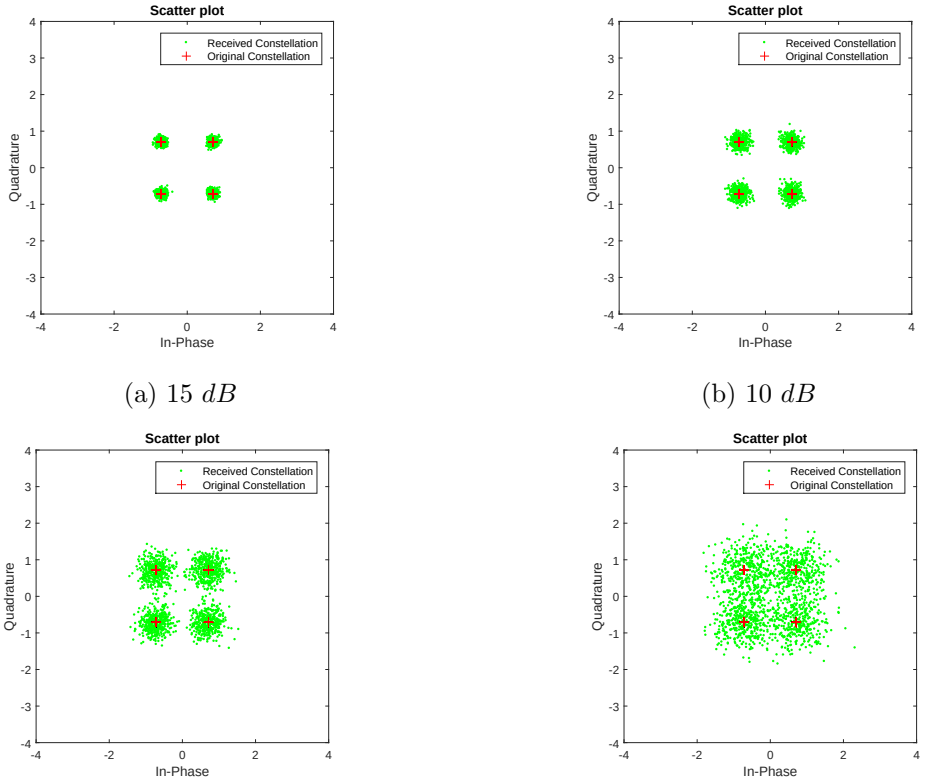

(a) 15 dB (b) 10 dB

(c) 5 dB (d) -5 dB

Figure 4.8: Same constellations after matched filtering is applied.

4.3 Linear Equalization and Matched Filtering

This last simulation aims to join the linear equalization and the matched filtering to solve the impairments resulting of a propagation affected by GVD and ASE, respectively. Thereby, the same set-up from Section 3.3 in order to apply both filters $H_1(\omega)$ and $H_2(\omega)$, resulting of an only one filter $H_3(\omega)$ that joins their responses. The MATLAB code regarding this simulation can be consulted in Appendix C.6.

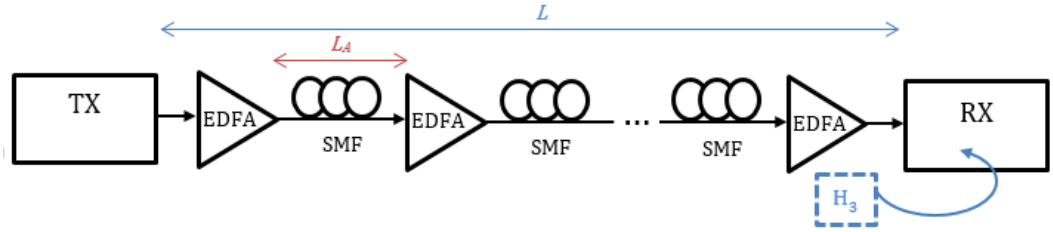

Figure 4.9: Block diagram of a transmission system whose receiver performs linear equalization and matching filtering simultaneously.

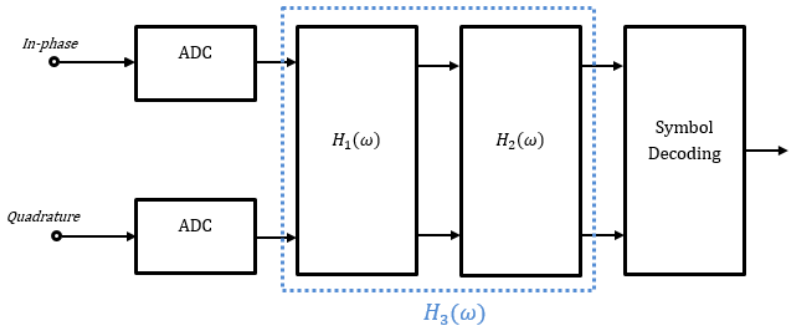

Figure 4.10: Block diagram of the receiver in detail, containing the filter $H_3(\omega)$.

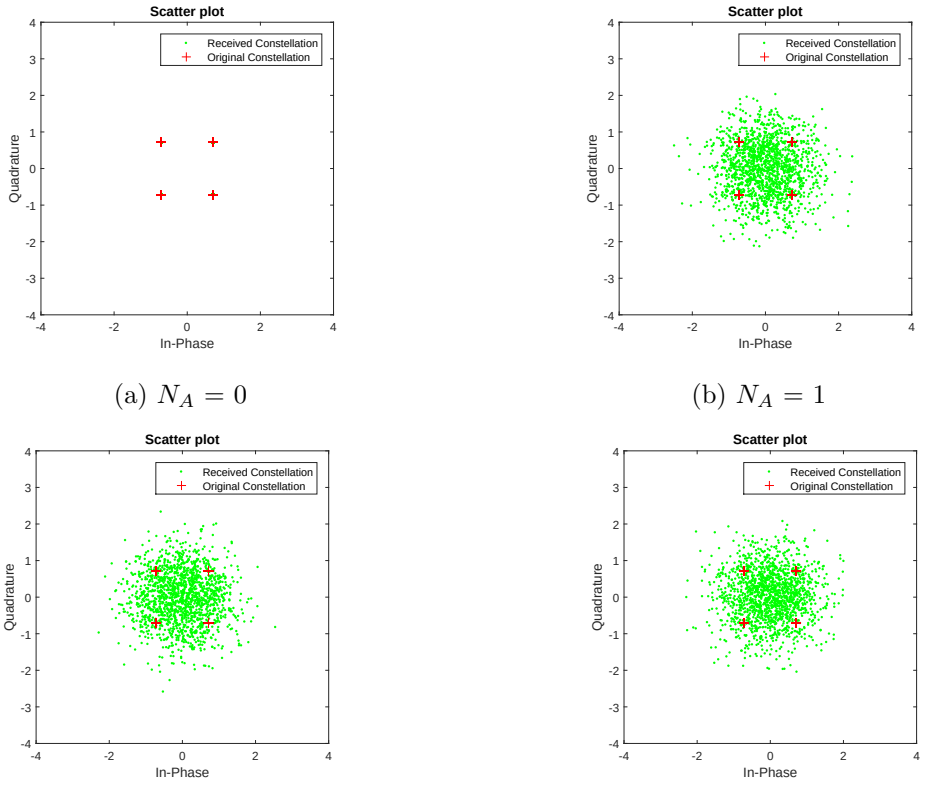

(a) $N_A = 0$

(b) $N_A = 1$

(c) $N_A = 10$

(d) $N_A = 50$

Figure 4.11: Constellations resulting of different number of regenerators before linear equalization and matched filtering are applied.

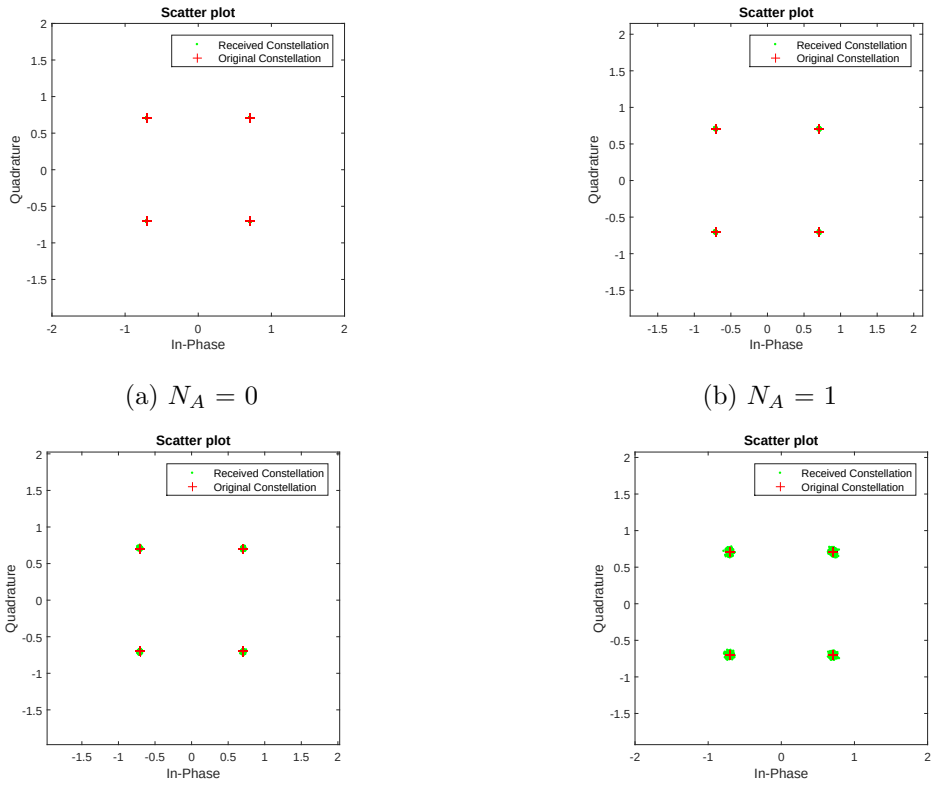

(a) $N_A = 0$ (b) $N_A = 1$

(c) $N_A = 10$ (d) $N_A = 50$

Figure 4.12: Same constellations after linear equalization and matched filtering are applied.

4.4 Conclusions

In a parallel approach relatively to the previous Chapter, there were used the same three propagation scenarios in order to extract the undesired effects from the received signal. Observing the results, it is possible to conclude that the chromatic dispersion effect is possible to eliminate completely, unlike the noise effect. This is because the GVD is given by a linear and deterministic model and for compensate its response, the solution is simple as use an inverse model of the propagation. In the case of the white Gaussian noise, it is impossible to predict its model once it is random, then the compensation is performed by an approximate inverse model of the propagation, i.e. by a matched filter. So when both effects are present in a propagation the solution can be the application of a third filter to the received signal, which is proposed in the Section 4.3. This digital filter joins the linear equalization and the matched filtering responses.

Chapter 5

Conclusions

Fibre impairments severely impacts the performance of high-speed optical transmission systems, as it is affirmed in [2]. The current dissertation aims to demonstrate that fact through different simulations and under different conditions. It aims to demonstrate DSP solutions to solve those impairments likewise. Focusing on the GVD impact, the main target throughout the work was to understand this optical fibre phenomenon in order to mitigate it combined with other channel constraints, such as ASE. The solution approach consisted of linear equalization, proving that using only linear filtering, given an ideal system, it is possible to retrieve the transmission system performance totally.

As object of study, a QPSK coherent transmission system was used with ideal characteristics, i.e. with no components attenuation and with no external noise. The fact of the transmission system being coherent is related to the detection of the signal phase beyond the signal amplitude, which allows receiving both components in-phase and quadrature differentiated. Each block of the transmission system as well as the reception system was studied in detail before proceeding to any simulation. That study allowed taking the knowledge of the system into a more precise level and simulate it closely from the reality, but also suitable in the ideal model. In the case of the *pulse shaper* simulation, for instance, the rolloff factor and also the number of spans must be adjusted to the ideal conditions values. The rolloff was set to the minimum value and the number of spans was set to the maximum value respecting a computational effort limit.

Regarding the propagation channel, a linear model of GVD was used for simulation purposes. The three propagations simulated in the Chapter 3 yielded a signal whose symbols distribution tends to a normal distribution. Those results allow concluding whether chromatic dispersion whether noise causes a similar behaviour into the propagated signal. However, the signal retrieval process for both cases was not successful in the same way. While the GVD is a deterministic phenomenon, and even representable by a linear model, the noise is ran-

dom and unpredictable. This statement was proved in the Chapter 4 using the same three propagations than before. The CD effect can be completely mitigated using an equalizer that corresponds to a filter with an inverse response of the linear model for GVD, which is known in advance. In the case of the noise effect, the best solution is filtering the received signal with a matched filter based on its response. Throughout the simulations was still proved that the overlapping of the two effects generates independent distributions into the received signal.

5.1 Future Work

Once the current dissertation focused on the theory related to digital chromatic dispersion equalization, it makes sense that the next step be a more practical approach on the subject. So the following topics list should be a proposal for future work:

- Complete and test the simulation environment developed in C++;
- Implementation of the digital chromatic dispersion equalization in hardware language;
- Validation of the hardware implementation offline for a system at 100 Gb/s;
- Validation of the hardware implementation in real-time (FPGA) for a system at 10 Gb/s.

Bibliography

[1] A. Chralyvy, "The coming capacity crunch," in *ECOC09 - 35th European Conference on Optical Communication*, p. 1, Sept. 2009.

[2] P. G. Agrawal, *Fiber-optic communication systems.* A John Wiley & Sons, third ed., 2002.

[3] S. J. Savory, "Digital filters for coherent optical receivers," *Optics Express*, vol. 16, no. 2, pp. 804–817, 2008.

[4] F. Guiomar, C. Rodrigues, A. Pinto, and P. Mão-Cheia, "Transmissão e recepção coerente a 40 Gb/s e 100 Gb/s," *Saber & Fazer Telecomunicações*, no. 02, pp. 128–133, 2011.

[5] K. Kikuchi, *Coherent Optical Communications: Historical Perspectives and Future Directions*, vol. 6, ch. 2, pp. 11–50. Springer, Jan. 2010.

[6] O. E. DeLange, "Wide-band optical communication systems: Part ii —frequency-division multiplexing," *Proceedings of the IEEE*, vol. 58, pp. 1683–1690, Oct. 1970.

[7] T. Okoshi and K. Kikuchi, "Frequency stabilisation of semiconductor lasers for heterodyne-type optical communication systems," *Electronics Letters*, vol. 16, pp. 179–181, Feb. 1980.

[8] F. Favre and D. LeGuen, "High frequency stability of laser diode for heterodyne communication systems," vol. 16, pp. 709–710, 1980.

[9] S. Norimatsu and K. Iwashita, "Damping factor influence on linewidth requirements for optical PSK coherent detection systems," *Journal of Lightwave Technology*, vol. 11, pp. 1226–1233, July 1993.

[10] K.-P. Ho, *Phase-Modulated Optical Communication Systems.* Springer, 2005.

[11] J. M. Kahn and K.-P. Ho, "Spectral efficiency limits and modulation/detection techniques for DWDM systems," *Selected Topics in Quantum Electronics, IEEE Journal of*, vol. 10, no. 2, pp. 259–272, 2004.

[12] S. Tsukamoto, D.-S. Ly-Gagnon, K. Katoh, and K. Kikuchi, "Coherent demodulation of 40-Gbit/s polarization-multiplexed QPSK signals with 16-GHz spacing after 200-km transmission," in *Optical Fiber Communication Conference, 2005. Technical Digest. OFC/NFOEC*, vol. 6, pp. 3–pp, IEEE, 2005.

[13] G. Keiser, *Optical fiber communication*. McGraw-Hill, third ed., 2000.

[14] P. M. Becker, A. A. Olsson, and J. R. Simpson, *Erbium-doped fiber amplifiers: fundamentals and technology*. Academic press, 1999.

[15] A. H. Gnauck, R. Tkach, A. Chraplyvy, and T. Li, "High-capacity optical transmission systems," *Journal of Lightwave Technology*, vol. 26, no. 9, pp. 1032–1045, 2008.

[16] R. Griffin and A. Carter, "Optical differential quadrature phase-shift key (ODQPSK) for high capacity optical transmission," in *Optical Fiber Communication Conference and Exhibit, 2002. OFC 2002*, pp. 367–368, IEEE, 2002.

[17] F. P. Guiomar, "Digital post-compensation of the optical channel," Master's thesis, University of Aveiro, 2009.

[18] G. P. Agrawal, *Lightwave technology: telecommunication systems*. John Wiley & Sons, 2005.

[19] E. Ip, A. Lau, D. Barros, and J. Kahn, "Coherent detection in optical fiber systems," *Optics express*, vol. 16, no. 2, pp. 753–791, 2008.

[20] F. Koyama and K. Iga, "Frequency chirping in external modulators," *Lightwave Technology, Journal of*, vol. 6, no. 1, pp. 87–93, 1988.

[21] S. Shimotsu, S. Oikawa, T. Saitou, N. Mitsugi, K. Kubodera, T. Kawanishi, and M. Izutsu, "Single side-band modulation performance of a $LiNbO_3$ integrated modulator consisting of four-phase modulator waveguides," *IEEE Photonics Technology Letters*, vol. 13, pp. 364–366, Apr. 2001.

[22] S. Jansen, B. Spinnler, I. Morita, S. Randel, and H. Tanaka, "100GbE: QPSK versus OFDM," *Optical Fiber Technology*, no. 15, pp. 407–413, 2009.

[23] T. Eriksson, "Multidimensional modulation formats for coherent optical communication systems," Master's thesis, Chalmers University of Technology, 2014.

[24] T. F. Detwiler, S. M. Searcy, B. E. Basch, and S. E. Ralph, "Continuous phase modulation as an alternative to QPSK for 100 Gb/s optical links," in *Optical Fiber Communication (OFC), collocated National Fiber Optic Engineers Conference, 2010 Conference on (OFC/NFOEC)*, pp. 1–3, Mar. 2010.

[25] H. Sun, K.-T. Wu, and K. Roberts, "Real-time measurements of a 40 Gb/s coherent system," *Optics Express*, vol. 16, no. 2, pp. 873–879, 2008.

[26] T. Xu, G. Jacobsen, S. Popov, J. Li, A. T. Friberg, and Y. Zhang, "Digital chromatic dispersion compensation in coherent transmission system using a time-domain filter," in *Communications and Photonics Conference and Exhibition (ACP), 2010 Asia*, pp. 132–133, Dec. 2010.

[27] S. J. Savory, "Digital coherent optical receivers: algorithms and subsystems," *Selected Topics in Quantum Electronics, IEEE Journal of*, vol. 16, no. 5, pp. 1164–1179, 2010.

[28] E. Ip and J. M. Kahn, "Digital equalization of chromatic dispersion and polarization mode dispersion," *Journal of Lightwave Technology*, vol. 25, pp. 2033–2043, Aug. 2007.

[29] G. Goldfarb and G. Li, "Chromatic dispersion compensation using digital IIR filtering with coherent detection," *Photonics Technology Letters, IEEE*, vol. 19, no. 13, pp. 969–971, 2007.

[30] N. Benvenuto and G. Cherubini, *Front Matter*. Wiley Online Library, 2002.

[31] B. Spinnler, F. Hauske, and M. Kuschnerov, "Adaptive equalizer complexity in coherent optical receivers," in *Optical Communication, 2008. ECOC 2008. 34th European Conference on*, pp. 1–2, IEEE, 2008.

[32] B. Widrow, S. D. Stearns, and J. C. Burgess, "Adaptive signal processing," *The Journal of the Acoustical Society of America*, vol. 80, no. 3, pp. 991–992, 1986.

[33] D. N. Godard, "Self-recovering equalization and carrier tracking in two-dimensional data communication systems," *Communications, IEEE Transactions on*, vol. 28, no. 11, pp. 1867–1875, 1980.

[34] B. Le Nguyen, "Matlab simulink simulation platform for photonic transmission systems," *Int'l J. of Communications, Network and System Sciences*, 2009.

[35] M. Jeruchim, P. Balaban, and K. Shanmugan, *Simulation of Communication Systems*, ch. 3, pp. 284–285. Plenum, 1992.

[36] P. Alfke, "Efficient shift registers, lfsr counters, and long pseudo-random sequence generators." http://www.xilinx.com/bvdocs/appnotes/xapp052.pdf, 1998. Accessed: 28-03-2016.

[37] C. ©2005 New Wave Instruments, "Tables of m-sequence feedback taps." www.newwaveinstruments.com/resources/articles/m_sequence_linear_feedback_shift_register_lfsr.htm. Accessed: 04-04-2016.

[38] E. Cubukcu, "Root raised cosine filters and pulse shaping in communication systems." Engineering & Science Contract Group, NASA, 2012.

[39] A. R. R. Copyright ©2008, Eric Jacobsen, "Pulse shaping in single-carrier communication systems." www.dsprelated.com/showarticle/60.php. Accessed: 19-04-2016.

[40] M. Seimetz, *High-order modulation for optical fiber transmission*, vol. 143. Springer, 2009.

[41] C. ©2016 Fiber-Optics.Info, "Fiber dispersion - chromatic dispersion." www.fiber-optics.info/articles/fiber_dispersion. Accessed: 23-02-2016.

[42] F. Čertík, "Using matlab tools for simulation of the optical transmission medium," in *Technical Computing Bratislava 2012 [elektronický zdroj]: 20th Annual Conference Proceedings. Bratislava, 7.11*, 2012.

[43] C. ©2014 ThorLabs, "Dispersion compensating fiber." http://www.thorlabs.com/NewGroupPage9_PF.cfm?ObjectGroup_ID=5719. Accessed: 24-05-2016.

[44] C. ©2000-2016 Optoplex Corporation, "90-degree optical hybrid." http://www.optoplex.com/Optical_Hybrid.htm. Accessed: 27-04-2016.

[45] P. Poggiolini, G. Bosco, A. Carena, V. Curri, and F. Forghieri, "Performance evaluation of coherent WDM PS-QPSK (HEXA) accounting for non-linear fiber propagation effects," *Opt. Express*, vol. 18, pp. 11360–11371, May 2010.

[46] M. Benssalah and M. Djeddou, "Implementation of synchronization algorithms, carrier phase recovery and symbol timing recovery, on a digital signal processor," in *Signals, Circuits and Systems, 2009. ISSCS 2009. International Symposium on*, pp. 1–4, July 2009.

[47] M. Moeneclaey and G. de Jonghe, "ML-oriented NDA carrier synchronization for general rotationally symmetric signal constellations," *IEEE Transactions on Communications*, vol. 42, pp. 2531–2533, Aug. 1994.

[48] L. Litwin, "Matched filtering and timing recovery in digital receivers," *RF design*, vol. 24, no. 9, pp. 32–49, 2001.

[49] N. Stojanovic, F. N. Hauske, C. Xie, and M. Chen, "Clock recovery in coherent optical receivers," in *Photonic Networks, 12 . ITG Symposium*, pp. 1–4, May 2011.

[50] F. J. Massey Jr., "The Kolmogorov-Smirnov Test for Goodness of Fit," *Journal of the American Statistical Association*, vol. 46, no. 253, pp. 68–78, 1951.

[51] B. R. Mahafza, *Radar Systems Analysis and Design Using MATLAB*, ch. Chapter 6, pp. 233–242. Chapman & Hall/CRC, 2 ed., 2005.

Appendix A

C++ Functions

The first Appendix regards the C++ functions implemented in the PRBS level, in order to add and validate features to it. All the three functions belong to the *BinarySource* class which corresponds to PRBS in the QPSK transmitter's programming code. Firstly, *validBitStream(int pLength, vector<char>& values)* aims the validation of the bitstream given by the user, verifying if its length matches the pattern length (also given by the user), if it contains only '0's and '1's and at least one '1'. Then *error(int errorType)* typifies one of the possible three errors described and, lastly *Log(char *message)* receives the error type, writing the matching error message in a log file, which is automatically created in current directory.

```
bool BinarySource :: validBitStream(int pLength, vector<char>& values)
{
        patternLength = pLength;

        int valuesSize = values.size();

        if (valuesSize != pLength) {
                if (valuesSize > pLength)
                        error(1);
                else
                        error(2);
                values.resize(pLength + 1);
                for (int j = valuesSize; j < pLength + 1; j++)
                        values[j] = '0';
        }

        bool one = false;
        for (int i = 0; i < pLength; i++){
                if (values[i] != '0' && values[i] != '1') {
                        error(3);
```

```
                        return false;
                }
                if (values[i] == '1')
                        one = true;
        }
        if (!one)
                error(4);

        return one;
};
```

```
void BinarySource :: error(int errorType)
{
        string mError;

        switch (errorType){
        case 1:
                mError = "WARNING: Bit string length greater than pattern
length! Last bit values are discarded.";
                break;
        case 2:
                mError = "WARNING: Bit string length smaller than pattern
length! ZERO bit value is added at the end.";
                break;
        case 3:
                mError = "WARNING: Bit values must be ZERO or ONE! Bit values
changed to '100...'";
                break;
        case 4:
                mError = "WARNING: At least one bit must have the value ONE!
Bit values changed to '100...'";
                break;
        }

        std::vector<char> message(mError.begin(), mError.end());
        Log(&*message.begin());
        Log("\n");
};
```

```
# define LOGFILE "gl.log"      // all Log(); messages appended to this file

extern bool LogCreated = false;

void BinarySource :: Log(char *message)
{
```

```
        FILE *file;

        if (!LogCreated) {
                file = fopen(LOGFILE, "w");
                LogCreated = true;
        }
        else
                file = fopen(LOGFILE, "r");

        if (file == NULL) {
                if (LogCreated)
                        LogCreated = false;
                return;
        }
        else
        {       fputs(message, file);
                fclose(file);
        }

        if (file)
                fclose(file);
};
```

Appendix B

MATLAB Functions: PRBS

This second Appendix presents the MATLAB functions implemented in order to validate the sequences resulting of the PRBS block using the QPSK transmitter's simulation environment. Therefore, these functions may read an *'S1.sgn'*, yielded by C++ code, and require the pattern length which must match the pattern length used to generate the signal in C++.

The first function, *PRBSTest()*, validates the existence of the whole bit combinations within a sequence (all zeros' sequence not included). The second function, *PeriodicityTest()*, validates the periodicity of the sequence, i.e. if the sequence is repeating over the same period. Finally, *OpenBinarySignal(fileName, dataLength)* is an auxiliary function of both that may convert the *'.sgn'* into a MATLAB vector.

```
function [ ] = PRBSTest( ~ )

PATH = 'c:\Users\Utilizador\Desktop\signals\';

m = input('Insert the pattern length: ');

periodLength = 2^m-1;
dataLength = periodLength+m-1;

% it opens the signal and loads it for dataBinary vector
dataBinary = OpenBinarySignal([PATH 'S1.sgn'],dataLength);

confirVector = int8(zeros(1,periodLength));
for k=1:periodLength
        aux = dataBinary(k:k+m-1);
        dec = 0;
        for l=1:m
                dec=dec+aux(l)*2^(m-l);
        end
```

```
        if (dec > 0) \&\& (dec<=periodLength)
                confirVector(dec)=1;
        end
end

if (sum(confirVector)==periodLength) && (length(confirVector)==periodLength)
        disp('OK!');
else
        disp('Wrong!')
end

save dataBinary

end
```

```
function [ ] = PeriodicityTest( ~ )

PATH = 'c:\Users\Utilizador\Desktop\signals\';

m = input('Insert the pattern length: ');

periodLength = 2^m-1;
dataLength = periodLength+m-1;

% it opens the signal and loads it for dataBinary vector
dataBinary = OpenBinarySignal([PATH 'S1.sgn'],2*dataLength);

decim=zeros(1,2*periodLength);

for i=1:(2*periodLength)
        aux = dataBinary(i:i+m-1);
        dec = 0;
        for l=1:m
                dec=dec+aux(l)*2^(m-l);
        end
        decim(i)=dec;
end

count = 0;
for j=1:periodLength
        if decim(j) == decim(j+periodLength)
                count=count+1;
        end
end
```

```
if count == periodLength
        disp('Periodic');
else
        disp('Non periodic');
end

end
```

```
function data = OpenBinarySignal(fileName,dataLength)

% Open file
fid = fopen(fileName);

[~, ~, ~, ~] = readSignalHeader(fid);

data = fread(fid, dataLength,'uint32');

fclose(fid);

end
```

Appendix C

MATLAB Scripts Code: End-to-End Simulations

Each Section of this Appendix contains the MATLAB script code for each simulation set-up of both Chapters 3 and 4, as the titles indicate.

C.1 *Propagation with CD and without Noise*

```
%%%%%%%%%%%%%%%%%%%%%%%%%%%%%% Binary Source %%%%%%%%%%%%%%%%%%%%%%%%%%%%%%
M = 4;                          % Number of symbols
phOffset = pi/4;                % Phase offset
k = log2(M);                    % Number of bits per symbol
numBits = 1e5;                  % Number of bits to process
SymbolRate = 28e9;              % Symbol rate

rng default                             % Default random number generator
dataIn = randi([0 1], numBits, 1);  % Generate vector of binary data

%%%%%%%%%%%%%%%%%%%%%%%%%%%%%% QPSK Mapper %%%%%%%%%%%%%%%%%%%%%%%%%%%%%%%%
dataInMatrix = reshape(dataIn, length(dataIn)/k, k); % Reshape into binary 4
dataSymbolsIn = bi2de(dataInMatrix);                 % Convert to integers

dataMod = pskmod(dataSymbolsIn, M, phOffset, 'Gray'); % QPSK mapping

%%%%%%%%%%%%%%%%%%%%%%%%%%%%%% Pulse Shaper (TX) %%%%%%%%%%%%%%%%%%%%%%%%%%%
numSPS = 32;                    % Oversampling factor
fs = SymbolRate*numSPS;         % Sample rate
span = 20000;                   % Filter span in symbols
rolloff = 0;                    % Roloff factor
```

```
rrcFilter = rcosdesign(rolloff, span, numSPS, 'sqrt');  % RRC
txSignal = upfirdn(dataMod, rrcFilter, numSPS, 1);      % Upsample & filter

%%%%%%%%%%%%%%%%%%%%%% Optical Fibre (CD effect) %%%%%%%%%%%%%%%%%%%%%%
lambda = 1550*1e-9;                         % m
c = 299792458;                              % m/s
D = 17*1e-6;                                % s/nm/m
L = [0 1e3 10e3 100e3 1000e3];              % m

for v=1:length(L)

        tx = fftshift(fft(txSignal));   % Convert to frequency domain
        N = length(txSignal);
        f= -fs/2:fs/N:fs/2-fs/N;

        H_c = exp((1i*2*pi*D*L(v)*lambda^2*f.^2)/c); % CD frequency response
        rx = transpose(H_c).*tx;
        rxSignal = ifft(ifftshift(rx)); % Convert to time domain

        %%%%%%%%%%%%%%%%%%%%%% Bessel Low-Pass Filter %%%%%%%%%%%%%%%%%%%%%%
        Bandwidth = 200e9;
        [B,A] = besself(1,Bandwidth);
        H_bessel = freqz(B,A,length(rxSignal),'whole');
        LowPass_Filter = fftshift(abs(H_bessel));
        LPF_shifted = LowPass_Filter.*fftshift(fft(rxSignal));
        rxFilt = ifft(ifftshift(LPF_shifted));

        %%%%%%%%%%%%%%%%%%%%%% Pulse Shaper (RX) %%%%%%%%%%%%%%%%%%%%%%
        rxSignalFilt = upfirdn(rxFilt,rrcFilter,1,numSPS);% Downsample & filter
        rxSignalFilt = rxSignalFilt(span+1:end-span);    % Account for delay

        %%%%%%%%%%%%%%%%%%%%%% QPSK Demapper %%%%%%%%%%%%%%%%%%%%%%
        dataSymbolsOut=pskdemod(rxSignalFilt,M,phOffset,'Gray');% QPSK demapp.

        dataOutMatrix = de2bi(dataSymbolsOut,k);% Convert symbols into binary
        dataOut = dataOutMatrix(:);             % Return data in column vector

end
```

C.2 *Propagation with Noise and without CD*

```
%%%%%%%%%%%%%%%%%%%%%%%%%%%%%% Binary Source %%%%%%%%%%%%%%%%%%%%%%%%%%%%%%
...

%%%%%%%%%%%%%%%%%%%%%%%%%%%%%% QPSK Mapper %%%%%%%%%%%%%%%%%%%%%%%%%%%%%%%
...

%%%%%%%%%%%%%%%%%%%%%%%%%%%%%% Pulse Shaper (TX) %%%%%%%%%%%%%%%%%%%%%%%%%%%%%%
...

%%%%%%%%%%%%%%%%%%%%%%%%%%%%%% AWGN (Noise effect) %%%%%%%%%%%%%%%%%%%%%%%%%%%%%%
EbNoVector = [-10 -5 0 5 10];

for v = 1:length(EbNoVector)
        EbNo = EbNoVector(v);
        snr = EbNo + 10*log10(k) - 10*log10(numSPS);      % Signal noise ratio
        rxSignal = awgn(txSignal, snr, 'measured');       % AWGN channel

        %%%%%%%%%%%%%%%%%%%%%%%% Bessel Low-Pass Filter %%%%%%%%%%%%%%%%%%%%%%%%
        ...

        %%%%%%%%%%%%%%%%%%%%%%%% Downsample (ADC) %%%%%%%%%%%%%%%%%%%%%%%%
        rxDnSignal = upfirdn(rxFilt,1,1,numSPS);     % Downsample
        rxSignal = rxDnSignal(1:end-span);           % Account for delay

        %%%%%%%%%%%%%%%%%%%%%%%% QPSK Demapper %%%%%%%%%%%%%%%%%%%%%%%%
        ...
end
```

C.3 *Propagation with CD and Noise*

```
%%%%%%%%%%%%%%%%%%%%%%%%%%%% Binary Source %%%%%%%%%%%%%%%%%%%%%%%%%%%%
...
%%%%%%%%%%%%%%%%%%%%%%%%%%%% QPSK Mapper %%%%%%%%%%%%%%%%%%%%%%%%%%%%%
...
%%%%%%%%%%%%%%%%%%%%%%%%%%%% Pulse Shaper (TX) %%%%%%%%%%%%%%%%%%%%%%%%%
...
%%%%%%%%%%%%%%%%%%%%%%%%%%%% Optical Channel %%%%%%%%%%%%%%%%%%%%%%%%%%%
D = 17*1e-6;                                % s/nm/m
L = [0 100e3 500e3 1000e3 5000e3];          % Total length
La = 100e3;                                 % Span length
alpha = 0.2e-3;                             % Loss coefficient
hP = 6.62607004*1e-34;                      % Planck constant
nsp = 1;                                    % Spontaneous emission factor
lambda = 1550*1e-9;                         % m
c = 299792458;                              % m/s

for v=1:length(L)
        tx = fftshift(fft(txSignal));       % Convert to frequency domain
        N = length(txSignal);
        f=-fs/2:fs/N:fs/2-fs/N;
        Hc = transpose(exp((1i*2*pi*D*L(v)*lambda^2*f.^2)/c));
        rx = Hc.*tx;
        rxSignal = ifft(ifftshift(rx));     % Convert to time domain

        Na = L(v)/La;                       % Number of EDFAs
        gain = 10^(alpha*La/10);            % Linear gain
        NSD = Na*(gain - 1)*c/lambda*hP*nsp;% Noise spectral density
        N_optical_power(u) = 2*NSD*fs;      % Linear noise
        noise_I = sqrt(N_optical_power/2)*randn(length(txSignal),1);
        noise_Q = sqrt(N_optical_power/2)*randn(length(txSignal),1);
        noise = noise_I + 1i * noise_Q;
        rxSignal = rxSignal + noise;

        %%%%%%%%%%%%%%%%%%%%%% Bessel Low-Pass Filter %%%%%%%%%%%%%%%%%%%%%%
        ...
        %%%%%%%%%%%%%%%%%%%%%% Pulse Shaper (RX) %%%%%%%%%%%%%%%%%%%%%%%%%
        ...
        %%%%%%%%%%%%%%%%%%%%%% QPSK Demapper %%%%%%%%%%%%%%%%%%%%%%%%%%%%
        ...
end
```

C.4 *CD Equalization of a Propagation without Noise*

```
%%%%%%%%%%%%%%%%%%%%%%%%%%%%%% Binary Source %%%%%%%%%%%%%%%%%%%%%%%%%%%%%%
...

%%%%%%%%%%%%%%%%%%%%%%%%%%%%%% QPSK Mapper %%%%%%%%%%%%%%%%%%%%%%%%%%%%%%%
...

%%%%%%%%%%%%%%%%%%%%%%%%%%%%%% Pulse Shaper (TX) %%%%%%%%%%%%%%%%%%%%%%%%%%%%%%
...

%%%%%%%%%%%%%%%%%%%%%%%%%%%% Optical Fibre (CD effect) %%%%%%%%%%%%%%%%%%%%%%%%%%%%
...

for v=1:length(L)

        tx = fftshift(fft(txSignal));    % Convert to frequency domain
        N = length(txSignal);
        f= -fs/2:fs/N:fs/2-fs/N;

        H_c = exp((1i*2*pi*D*L(v)*lambda^2*f.^2)/c); % CD frequency response
        rx = transpose(H_c).*tx;
        rxSignal = ifft(ifftshift(rx)); % Convert to time domain

        %%%%%%%%%%%%%%%%%%%%%%%% Bessel Low-Pass Filter %%%%%%%%%%%%%%%%%%%%%%%%
        ...

        %%%%%%%%%%%%%%%%%%%%%%%% Pulse Shaper (RX) %%%%%%%%%%%%%%%%%%%%%%%%
        rxSignalFilt = upfirdn(rxFilt,rrcFilter,1,1);    % RRC filter
        rxSignalFilt = rxSignalFilt(1+span/2*numSPS:end-span/2*numSPS);

        %%%%%%%%%%%%%%%%%%%%%%%% CD Equalizer (DSP) %%%%%%%%%%%%%%%%%%%%%%%%
        H1 = (1./Hc);
        rxSignalEq=ifft(ifftshift(H1.*fftshift(fft(rxSignalFilt))));
        rxSignalEq = upfirdn(rxSignalEq,1,1,numSPS);     % Downsample
        rxSignalEq = rxSignalEq(1+span/2:end-span/2);    % Account for delay

        %%%%%%%%%%%%%%%%%%%%%%%% QPSK Demapper %%%%%%%%%%%%%%%%%%%%%%%%
        ...

end
```

C.5 *Matched Filtering of a Propagation with Noise and without CD*

```
%%%%%%%%%%%%%%%%%%%%%%%%%%%%% Binary Source %%%%%%%%%%%%%%%%%%%%%%%%%%%%%
...

%%%%%%%%%%%%%%%%%%%%%%%%%%%%% QPSK Mapper %%%%%%%%%%%%%%%%%%%%%%%%%%%%%%
...

%%%%%%%%%%%%%%%%%%%%%%%%%%%%% Pulse Shaper (TX) %%%%%%%%%%%%%%%%%%%%%%%%%%
...

%%%%%%%%%%%%%%%%%%%%%%%%%%%%% AWGN (Noise effect) %%%%%%%%%%%%%%%%%%%%%%%%
EbNoVector = [-5 0 5 10 15];

for v = 1:length(EbNoVector)
        EbNo = EbNoVector(v);
        snr = EbNo + 10*log10(k) - 10*log10(numSPS);     % Signal noise ratio
        rxSignal = awgn(txSignal, snr, 'measured');      % AWGN channel

        %%%%%%%%%%%%%%%%%%%%%%% Bessel Low-Pass Filter %%%%%%%%%%%%%%%%%%%%%%
        ...

        %%%%%%%%%%%%%%%%%%%%%%% Matched Filter/RRC (DSP) %%%%%%%%%%%%%%%%%%%%%%
        H2 = rcosdesign(rolloff, span, numSPS, 'sqrt'); % RRC filter
        rxFiltSignal = upfirdn(rxFilt,H2,1,numSPS);      % Downsample & filter
        rxFiltSignal = rxFiltSignal(1+span:end-span);    % Account for delay

        %%%%%%%%%%%%%%%%%%%%%%% QPSK Demapper %%%%%%%%%%%%%%%%%%%%%%%%%%%%%%
        ...

end
```

C.6 *CD Equalization and Matched Filtering*

```
%%%%%%%%%%%%%%%%%%%%%%%%%%%%%% Binary Source %%%%%%%%%%%%%%%%%%%%%%%%%%%%%%
...

%%%%%%%%%%%%%%%%%%%%%%%%%%%%%% QPSK Mapper %%%%%%%%%%%%%%%%%%%%%%%%%%%%%%%
...

%%%%%%%%%%%%%%%%%%%%%%%%%%%%%% Pulse Shaper (TX) %%%%%%%%%%%%%%%%%%%%%%%%%%%%%%
...

%%%%%%%%%%%%%%%%%%%%%%%%%%%%%% Optical Channel %%%%%%%%%%%%%%%%%%%%%%%%%%%%%%%
for v = 1:length(L)

        tx = fftshift(fft(txSignal));    % Convert to frequency domain
        N = length(txSignal);
        f=-fs/2:fs/N:fs/2-fs/N;
        Hc = transpose(exp((1i*2*pi*D*L(v)*lambda^2*f.^2)/c));
        rx = Hc.*tx;
        rxSignal = ifft(ifftshift(rx));          % Convert to time domain

        Na = L(v)/La;                            % Number of EDFAs
        gain = 10^(alpha*La/10);                 % Linear gain
        NSD = Na*(gain - 1)*c/lambda*hP*nsp;     % Noise spectral density
        N_optical_power(u) = 2*NSD*fs;           % Linear noise
        noise_I = sqrt(N_optical_power/2)*randn(length(txSignal),1);
        noise_Q = sqrt(N_optical_power/2)*randn(length(txSignal),1);
        noise = noise_I + 1i * noise_Q;
        rxSignal = rxSignal + noise;

        %%%%%%%%%%%%%%%%%%%%%%% Bessel Low-Pass Filter %%%%%%%%%%%%%%%%%%%%%%%
        ...

        %%%%%%%%%% Digital Equalizer & Matched Filter (DSP) %%%%%%%%%%
        rxSignalFilt = upfirdn(rxFilt,H2,1,1);  % RRC filter
        rxSignalFilt = rxSignalFilt(1+span/2*numSPS:end-span/2*numSPS);
        rxSignalEq=ifft(ifftshift(H1.*fftshift(fft(rxSignalFilt))));
        rxSignalEq = upfirdn(rxSignalEq,1,1,numSPS);     % Downsample
        rxSignalEq = rxSignalEq(1+span/2:end-span/2);    % Account for delay

        %%%%%%%%%%%%%%%%%%%%%%% QPSK Demapper %%%%%%%%%%%%%%%%%%%%%%%%%%%%%%%
        ...
end
```